BRNO UNIVERSITY OF TECHNOLOGY

VYSOKÉ UČENÍ TECHNICKÉ V BRNĚ

FACULTY OF ELECTRICAL ENGINEERING AND COMMUNICATION

FAKULTA ELEKTROTECHNIKY A KOMUNIKAČNÍCH TECHNOLOGIÍ

DEPARTMENT OF RADIO ELECTRONICS

ÚSTAV RADIOELEKTRONIKY

METHODS OF NUMERICAL INVERSION OF LAPLACE TRANSFORMS FOR ELECTRICAL ENGINEERING AND THEIR APPLICATIONS

METODY NUMERICKÉ INVERZNÍ LAPLACEOVY TRANSFORMACE PRO ELEKTROTECHNIKU A JEJICH APLIKACE

ABRIDGED DOCTORAL THESIS

TEZE DISERTAČNÍ PRÁCE

AUTHOR
AUTOR PRÁCE
    Nawfal Al-Zubaidi R-Smith, MSc.

SUPERVISOR
ŠKOLITEL
    prof. Ing. Lubomír Brančík, CSc.

BRNO 2018

KEYWORDS

THE MANUSCRIPT OF DISSERTATION IS STORED AT

Department of Radio Electronics
Faculty of Electrical Engineering and Communication
Brno University of Technology
Technicka 3082/12
616 00 Brno
Czech Republic

Contents

INTRODUCTION

Numerical Inverse Laplace Transforms (NILT) methods are classified by researchers to be methods that are profoundly utilized in time-domain simulations, and they are broadly used in various scientific areas, for instance, applications that require the solution of ordinary differential equations or those dealing with partial differential equations [1–8]. Realizing and solving signal integrity issues, especially in high speed digital systems with sufficiently high-clock frequencies, is often related to the analytic solutions of mathematical governing equations. In such situations the Laplace transform '$\mathbf{L}\{\cdot\}$' is often used, due to its simplicity and effectiveness, to deal with different transient excitation functions (e.g. Dirac, Heaviside, periodic functions), and hence transforming the solution into a linear simplified mathematical description [2]. Primarily these transforms are very attractive in solving differential equations, which arise in fields such as automatics, control theory, and transient process in linear time invariant systems [3]. Nevertheless, the inevitable steps are to obtain the original result in the time domain which is considered to be the most difficult part and, in some situations, can be even impossible to obtain analytically [4], among which we can mention transcendental and/or irrational Laplace transforms. The NILT methods can therefore be a potential tool to overcome these complications by determining the original in a fast and accurate manner. Numerical inverse Laplace transform methods can be generally sorted according to the number of variables or dimensions that the method is derived upon, which can be categorized as follows [5–10]:

- One-dimensional NILT methods (1D NILT):
  Most of the NILT methods available in literature are considered to be one-dimensional methods; these methods are fundamental, especially for the solution of ordinary differential equations.
- Two-dimensional NILT methods (2D NILT):
  The two-dimensional methods are effective, and the need to use the 2D variables arise mainly for solving problems such as partial differential equations; for instance, solution of transmission line and related analysis.
- Multi-dimensional NILT methods (MNILT):
  Multi-dimensional methods are important for solving more complex systems, such as that for nonlinear circuit analysis.

Performing a research on one-dimensional NILT methods shows us that there exist multiple methods, mainly those that are usually related to a specific field of application and hence could be considered as limited methods. The different 1D-NILT methods differ from one another by their range of applicability, stability, accuracy and, last but not least, the speed of computation. The range of applications of a certain NILT method are usually difficult to anticipate without running some tests on the method and computing their absolute errors. Then, after having performed such tests, then it is possible to classify the method and decide on which field of application or 'type of functions' the specific NILT method performs best on. The second characteristic, the stability of the method, which is an important phenomenon of the numerical method, i.e. if a specific method is not stable on some type of function, then the method could lead to very absurd results; mathematically speaking, a reason for instability could be for example when the NILT algorithm is of a fractional form with a difference in the denominator, that could be, in some cases, equal to zero and then infinity is a result at that specific point. Generally, a stable method also means a wider range of application for the numerical method. The third characteristic to list is the accuracy of the method, or in other words, to have relatively small absolute error when performing error analysis for a NILT method. Finally, the computational speed of a NILT method; with the constant development in science and technology, time becomes a more important factor, and hence, the methods with a fast-computational time are preferred. The backbone of the NILT methods is the inverse Laplace transform (ILT) technique, as shown in (1) and (2), representing

the Laplace transform and its inversion; where s is the Laplace complex variable,

$$F(s) = \int_0^\infty f(t)e^{-st}dt, \tag{1}$$

$$f(t) = \frac{1}{2\pi j} \int_0^\infty F(s)e^{st}ds, \tag{2}$$

The Laplace transform is an effective tool used in science and engineering specially for solving differential equations or generally assisting in time-domain simulations for different applications; even though, the main difficulty is then inverting the Laplace domain solution back into real time domain, in simple cases it could be done by using the Laplace inverting tables; however, for more sophisticated applications, such as that for systems with distributed parameters, where transcendental or irrational types of functions are involved, then the inversion is very difficult or even impossible [1, 11]. In all of these mentioned cases, the NILT methods can play an efficient role in solving these quantities of interest. In research, there exist several one-dimensional NILT methods which are used for inverting functions of one variable; though much less attention was paid to higher dimensional-NILTs, mainly due to the non-existent closed form inversions [9, 12–14]. Therefore, multi-dimensional NILT methods are of our high interest due to the necessity to solve scientific quantities of concern in deterministic and stochastic models, those especially arising in the fields of electrical engineering, radio communications, and computer sciences [12].

1 DISSERTATION OBJECTIVES

The importance of the numerical inverse Laplace transforms (NILT) methods for 1D, 2D and n-dimensional inversion methods arises as for their large field of applications in science, physics, and chemistry and, especially for our field of focus, the electrical and electronics engineering field [8, 15, 16]. This brings us up to the open-ended question, could we develop a relatively universal NILT method with one or more variables that is verified to be stable and accurate enough for terms of electrical engineering? All this and more open issues will be addressed shortly. The emphasis, in this dissertation, is to characterize and study the current developed methods and to further devise a relatively universal, stable and accurate method which could be easily applied and implemented for electrical engineering applications, such as transmission lines analysis, multi-conductor lines or more sophisticated like non-linear circuit simulation [8, 16].

1.1 Theoretical basis analysis and comparative studies

   I. Research of the theoretical basis of the numerical inversion methods, review and comparative study of different developed NILT methods.
  II. The development of single-variable NILT methods and their successful program implementation.
 III. Categorization of the different methods with regard to their applicability on electrical engineering topics and their relevance to the scientific field.
 IV. Incorporation of fractional-order calculus in the different applications of NILT methods, e.g. fractional-order TL modeling and simulation using NILT method.

1.2 Multivariable integral transforms

   I. Research study of the theoretical basis of multivariable integral transforms, review of numerical methods of two and more variable inverse Laplace transformation methods, and development of their program codes.

II. Application of MNILT in electrical engineering field, and utilizing Volterra series theory with the possibility of its application into non-linear systems analysis.
III. Inclusion of fractional-order calculus for the applications of MNILT, e.g. fractional-order multiconductor transmission lines modeling and simulation.

1.3 Development of effective NILT techniques

I. Development of effective numerical techniques for the inversion of Laplace transforms of one-variable and multi-variables.
II. Integration of efficient acceleration techniques to the proposed NILT methods, which yield to result enhancements.
III. Development and implementation of the corresponding program codes.
IV. Error analysis and accuracy tests for each of the above mentioned cases.
V. Verification by successful application in linear and non-linear systems analysis.
VI. Incorporation of fractional-order elements for related NILT applications.
VII. Innovative approaches to the solution of PDE's describing lossy coupled multiconductor transmission lines (MTL).

2 1D HYPERBOLIC NILT METHOD

In this chapter, a potential method, which is relatively universal and has a desirable accuracy, is presented and described. An advantage of this method is that its accuracy can be improved simply without changing the algorithm but only on the cost of the computational time. In the following sections, the related error analysis is studied, afterwards, an enhancement to the proposed method is done by integrating several infinite series convergence accelerating algorithms, which improve the accuracy and computational time of the method. Moreover, the corresponding analysis and tests are shown by using relevant test functions of known originals.

2.1 Original proposed 1D hyperbolic-based NILT method

I. Principle formula and basic assumptions
The hyperbolic NILT method is based on approximating the Laplace transform definition Bromwich integral, [1, 5, 17, 18],

$$f(t) = \frac{1}{2\pi \mathrm{j}} \int_{c-\mathrm{j}\infty}^{c+\mathrm{j}\infty} F(s)\mathrm{e}^{st}ds, \tag{2.1}$$

where $s = c + \mathrm{j}\omega$, while considering the basic assumptions,
- $F(s)$ is regular for $\mathrm{Re}\{s\} > 0$,
- when $|s| \to \infty$ then $F(s) \to 0$, and
- $F^*(s) = F(s^*)$, where the symbol * represents the complex conjugate.

II. Recapitulation of original hyperbolic NILT
The Laplace transform's inverse kernel e^{st} in (2.1) can be approximated by two hyperbolic relations, namely

$$K_{sh}(st, a) = \frac{\mathrm{e}^a}{2\sinh(a - st)}, \tag{2.2}$$

$$K_{ch}(st, a) = \frac{\mathrm{e}^a}{2\cosh(a - st)}, \tag{2.3}$$

Henceforth, the reciprocal hyperbolic functions are expressed by the infinite sum of rational functions in $z = a - st$,

$$\frac{1}{\sinh z} = \frac{1}{z} + 2z \sum_{n=1}^{\infty} \frac{(-1)^n}{n^2\pi^2 + z^2}, \tag{2.4}$$

$$\frac{1}{\cosh z} = 2\pi \sum_{n=0}^{\infty} \frac{(-1)^n(n+0.5)}{(n+0.5)^2\pi^2 + z^2}. \tag{2.5}$$

Further, continuing the derivation with the successive application of the residual theorem and performing simple mathematical manipulations, described in more detail in [5], we obtain the following approximate formulae

$$f_{sh}(t, a) = \frac{e^a}{t}\left(\frac{1}{2}F\left(\frac{a}{t}\right) + \sum_{n=1}^{\infty}(-1)^n \mathrm{Re}\left\{F\left(\frac{a}{t} + \frac{nj\pi}{t}\right)\right\}\right), \tag{2.6}$$

$$f_{ch}(t, a) = \frac{e^a}{t}\sum_{n=1}^{\infty}(-1)^n \mathrm{Im}\left\{F\left(\frac{a}{t} + \frac{(n-0.5)j\pi}{t}\right)\right\}, \tag{2.7}$$

There exists an alternative way to express the hyperbolic functions, i.e. their definition exponential functions, (2.2) and (2.3) can be rearranged into the form of the sum of infinite geometric series, and hence, from that, the absolute errors of formulae (2.6) and (2.7) can be obtained, respectively, as listed bellow,

$$\varepsilon_{sh}(t, a) = \sum_{n=1}^{\infty} e^{-2na} f((2n+1)t), \tag{2.8}$$

$$\varepsilon_{ch}(t, a) = \sum_{n=1}^{\infty}(-1)^n e^{-2na} f((2n+1)t). \tag{2.9}$$

By performing several tests it is found that the arithmetic mean of both NILT approximations (2.6) and (2.7) results in an even more enhanced and accurate inversion algorithm, namely

$$f_{en}(t, a) = \frac{e^a}{2t}\left(\frac{1}{2}F\left(\frac{a}{t}\right) + \sum_{n=1}^{\infty}(-1)^n\left(\mathrm{Re}\left\{F\left(\frac{a}{t} + \frac{nj\pi}{t}\right)\right\}\cdots\right.\right.$$
$$\left.\left. + \mathrm{Im}\left\{F\left(\frac{a}{t} + \frac{(n-0.5)j\pi}{t}\right)\right\}\right)\right), \tag{2.10}$$

the absolute error of (2.10) can be analytically obtained

$$\varepsilon_{en}(t, a) = \sum_{n=1}^{\infty} e^{-4na} f((4n+1)t). \tag{2.11}$$

2.1.1 Generalization of the 1D hyperbolic NILT method

The work, presented in reference [1], describes the possibility for a generalization of the method for a better accuracy, which basically allows to increase the accuracy of the method by the reduction of the integration step with the possibility to predict the absolute limit error [17]. This alternative approach to improve the accuracy provides a broader range of application to the hyperbolic NILT method, with the ability of optimizing the free parameter a to attain a marginally absolute error. Mainly, the integration step is reduced by $\Omega = \pi/mt$, where m is an integer, while maintaining the parameter c as it was originally defined [1].

2.1.2   Integration of infinite series convergence acceleration techniques

With the motivation to reduce the 'static' error effect and further enhance the proposed hyperbolic NILT original method, the idea of adapting some infinite series convergence acceleration techniques is proposed; and then after several tests, using the Matlab programming language, their performance on the hyperbolic NILT method and compare their results. Specific convergence acceleration techniques are available and suitable to be integrated with the proposed method. Namely, the techniques incorporated to the hyperbolic NILT method are: the Euler transform, the quotient-difference algorithm of Rutishauser and the epsilon algorithm of Wynn; this will be shown in the following sections. In practice, the computation of formula (2.10) is done as follows; first it can be formally rewritten as a combination of three parts, i.e. an initial, a finite sum and an infinite sum,

$$f_{en}(t,a) = \frac{e^a}{2t}\left(\frac{1}{2}F\left(\frac{a}{t}\right) + \sum_{n=1}^{n_{sum}}(\cdots) + \sum_{n=n_{sum}+1}^{\infty}(\cdots)\right), \tag{2.12}$$

the initial part and the finite part are computed normally as they are, whereas the infinite part, in practice, can be computed up to a relatively high number of terms, e.g. 500 terms or higher. Nevertheless, by adapting suitable infinite series convergence acceleration techniques, the number of computed terms can be highly reduced, and in the same time, providing an increase in the accuracy of the method's results, saving valuable memory storage, and reducing the computational time.

I. By means of the Euler transform:
The infinite series in (2.10) for practical computation is truncated into a finite number of terms n_{sum}, as shown in (2.12), which leads to a decrease in the accuracy of the inversion result. To suppress this effect the Euler transform (ET) is incorporated. The ET is a well-known technique for accelerating the convergence of infinite series [19]. This technique performs at its best for alternating infinite series [1,5,7]. Practically, the ET is applied after n_{sum} terms are computed numerically by the hyperbolic NILT algorithm then n_{eul} terms are added, but weighted by factors, namely

$$2^{(-n_{eul})}V_{(n_{eul}-k+1)}, \tag{2.13}$$

where $k = 1, 2, \ldots, n_{eul}$, and V_r is given by the recursive formula

$$V_{r+1} = V_r + \binom{n_{eul}}{r}, \ V_1 = 1. \tag{2.14}$$

The final result obtained is then added as a replacement to the infinite series part of (2.12). The Euler transform gives a high improvement on the proposed method, for both the accuracy and computational speed, as will be verified in following sections from the several performed simulation test results. Mainly, an improvement on the accuracy of the inversion, computational speed and less memory usage are achieved by introducing the Euler transform to the proposed hyperbolic NILT method. Hereon, the hyperbolic NILT method in conjunction with the Euler convergence acceleration technique is denoted as 'Hyp-Eul NILT'.

II. By means of the quotient-difference algorithm:
The quotient-difference algorithm (QdA) of Rutishauser is considered to be a highly stable and efficient acceleration method [20]. The QdA gives, under certain conditions, the roots as the limits of similar quotient sequences [21]; for a power series, this algorithm corresponds to a rational Padé approximation expressed as a continued fraction.
Practically, the infinite sum is computed up to n_{sum} number of terms and the QdA requires only $n_{qd} = 2P + 1$ additional terms above n_{sum} as input data. Namely, considering (2.10)

<div align="center">8</div>

the 'finite' term is computed normally as it is, whereas, the 'infinite' term is rearranged, for simplicity, as follows

$$\sum_{n=1}^{\infty} (-1)^n \left[\operatorname{Re}\left\{ F\left(\frac{a + \mathrm{j}n\pi}{t} \right) \right\} + \operatorname{Im}\left\{ F\left(\frac{a + \mathrm{j}(n - 0.5)\pi}{t} \right) \right\} \right]$$

$$= \sum_{n=1}^{\infty} z^n Q_n \approx \sum_{n=1}^{n_{sum}} z^n Q_n + y(z, P), \qquad (2.15)$$

where $z = -1$, Q_n is the expression in the square brackets, and the term $y(z, P)$ represents the result of the QdA applied on additional n_{qd} terms of the residual original infinite series,

$$y(z, P) = \cfrac{d_0}{1 + \cfrac{d_1 z}{1 + \cfrac{d_2 z}{1 + \cfrac{d_3 z}{1 + \cdots + d_{2P}}}}} \;, \qquad (2.16)$$

which considerably improves the precision of the results. In order to evaluate the coefficients $d_n = 0, \cdots, 2P$, a clear demonstration can be based on the quotient-difference algorithm diagram illustrated in Fig. 2.1, [20,22]. The coefficients $d_n = 0, 1, \cdots, 2P$ in (2.16) are based

$$
\begin{array}{cccccc}
e_0^{(0)} & & & & & \\
 & q_1^{(0)} & & & & \\
e_0^{(1)} & & e_1^{(0)} & & & \\
 & q_1^{(1)} & & q_2^{(0)} & & \\
e_0^{(2)} & & e_1^{(1)} & & e_2^{(0)} & \\
 & q_1^{(2)} & & q_2^{(1)} & & \\
e_0^{(3)} & & e_1^{(2)} & & & \\
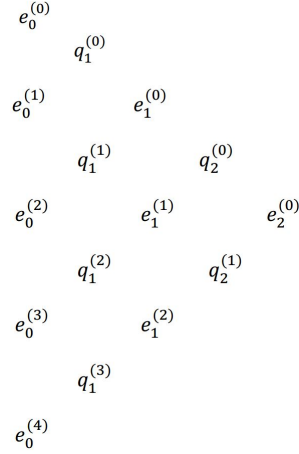 & q_1^{(3)} & & & & \\
e_0^{(4)} & & & & & \\
\end{array}
$$

Fig. 2.1: The quotient-difference algorithm's lozenge diagram.

on the QdA lozenge diagram, see Fig. 2.1, which is computed by the following process; the first two columns are filled by

$$e_0^{(k)} = 0, \; k = 0, \cdots, 2P, \qquad (2.17)$$

$$q_1^{(k)} = \frac{Q_{k+1}}{Q_k}, \; k = 0, \cdots, 2P - 1, \qquad (2.18)$$

the consequent columns are formed by the following relations for $r = 1, \cdots, P$,

$$e_r^{(k)} = q_r^{(k+1)} - q_r^{(k)} + e_{r-1}^{(k+1)}, \; k = 0, \cdots, 2P - 2r, \qquad (2.19)$$

for $r = 2, \cdots, P$,

$$q_r^{(k)} = \frac{q_{r-1}^{(k+1)} e_{r-1}^{(k+1)}}{e_{r-1}^{(k)}}, \; k = 0, \cdots, 2P - 2r - 1, \qquad (2.20)$$

now it is possible to obtain the coefficients $d_n = 0, 1, \ldots, 2P$ by the following relations

$$d_0 = Q_0, \ d_{2m-1} = -q_m^{(0)}, \ d_{2m} = -e_m^{(0)}, \ m = 1, \cdots, P. \tag{2.21}$$

A practical computation to get the solution of $y(z, P)$ can be done by processing the following recursive formulae,

$$A_n(z) = A_{n-1}(z) + d_n z A_{n-2}(z), \tag{2.22}$$

$$B_n(z) = B_{n-1}(z) + d_n z B_{n-2}(z), \tag{2.23}$$

where $n = 1, \cdots, 2P$, and the initial coefficients given are $A_{-1} = 0, B_{-1} = 1, A_0 = d_0$, and $B_0 = 1$. Finally, the continued fraction (2.16) can be given as $y(z, P) = A_{2P}(z)/B_{2P}(z)$, for any z. The simulation of the quotient-difference algorithm adaption to the proposed NILT method is performed in the universal Matlab programming language.

III. By means of the ε-algorithm of Wynn:

The next convergence acceleration technique integrated is the ε-algorithm of Wynn [23]. The ε-algorithm is categorized as a nonlinear technique used to accelerate the convergence of infinite series and iterations. It has also been used to obtain useful results from divergent series/iterations and to assist in the solution of differential and integral equations [23, 24]. The process followed to adapt the ε-algorithm to the 1D hyperbolic NILT method is theoretically similar to the QdA process, i.e. using a few number terms n_{eps} above n_{sum} which are used as input data to the ε-algorithm. In its turn, the ε-algorithm samples the additional terms and extrapolates them by fitting them to a polynomial multiplied by a decaying exponential [25]. Mathematically, the ε-algorithm can be described first by illustrating the lozenge diagram of the method, illustrated in Fig. 2.2. The diagram describes the case where $P = 2$, such that the total number of additional terms used is $2P + 1$ terms. To obtain the values of the lozenge diagram symbols used the following formulas will be
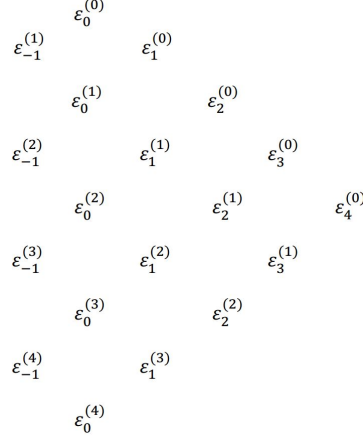

Fig. 2.2: The ε-algorithm's lozenge diagram.

used [10, 24]. Namely, to construct the first column $\varepsilon_{-1}^{(k)} = 0, k = 1, \cdots, 2P$ is used. The initial term in the second column $\varepsilon_0^{(0)}$ represents the result of the truncated finite sum (2.12). Subsequently, the remaining entries of the second column represent partial sums computed recurrently by

$$\varepsilon_0^{(k)} = \varepsilon_0^{(k-1)} + F_{(n_{sum}+k)} z^k, \ k = 1, \ldots, 2P. \tag{2.24}$$

where $F_{n_{sum}}$ is the result of the finite part of (2.12) computed up to n_{sum} terms, and $z = -1$.

The following columns for $r = 1, \ldots, 2P$, are obtained by the formula

$$\varepsilon_r^{(k)} = \varepsilon_{r-2}^{(k+1)} + [\varepsilon_{r-1}^{(k+1)} - \varepsilon_{r-1}^{(k)}]^{-1}, \; k = 0, \ldots, 2P - r. \tag{2.25}$$

When finishing the recurrent steps according to (2.25) the sequence of successive approximations $\varepsilon_0^{(0)}$, $\varepsilon_2^{(0)}$, $\varepsilon_4^{(0)}$... is obtained. This sequence converges much faster than the original sequence of partial sums. The required result from the EA transform is the entry $\varepsilon_{2P}^{(0)}$. Nevertheless, the algorithm can be under instability if P is chosen too high, based on previous experiments $P = 2$ or $P = 3$ seem to be sufficient [10].

2.1.3 Experimental error analysis

In this section, an experimental error analysis is performed, with the intention to confirm the theoretical error analysis (2.11). Moreover, it is interesting to investigate the effect of the different acceleration techniques presented earlier on the proposed hyperbolic-NILT method, namely, these techniques are the Hyp-ε NILT, the Hyp-Qd NILT and the Hyp-Eul NILT. The test functions used, shown in Tab. 2.1, are chosen intentionally to be of different mathematical types, i.e. rational, irrational and transcendental functions with pre-known originals, to test the method's performance.

Tab. 2.1: List of test functions with their pre-known originals

	Functions in the Laplace domain	Original functions in the time domain
1	$F_1(s) = \frac{2 \cdot \omega^3}{[s^2 + \omega^2]^2}$	$f_1(t) = \sin(\omega t) - \omega t \cos(\omega t)$
2	$F_2(s) = \frac{e^{-\sqrt{s}}}{s}$	$f_2(t) = \mathrm{erfc}\left(\frac{1}{2\sqrt{t}}\right)$
3	$F_3(s) = \frac{1 - e^{-s}}{2s} e^{-s}$	$f_3(t) = 0.5$ if $1 \leq t \leq 2$, and 0 elsewhere .

The results of testing functions $(F_1 - F_3)$ in conjunction with their absolute error plots are displayed in Fig. 2.3 to Fig. 2.5 [26]. These results illustrate the inversions done by proposed accelerated NILT methods discussed above. Respective adapted acceleration techniques have been algorithmized in the Matlab language and were analyzed as for their accuracy, numerical stability and optimal choice of their parameters. Generally, the following statements can be conceived as for the hyperbolic NILT method; the quotient-difference is more numerically stable, mainly when compared to the epsilon algorithm, i.e. due to the mathematical structure of the epsilon algorithm, a probability exists that in the denominator two big numbers of near values are subtracted, which leads to the denominator to approach zero and hence cause some instability [24]. On the other hand, the Euler transform gives a high impact on the accuracy of the method's results, it can be clearly noticed by checking the absolute error in Fig. 2.3 to Fig. 2.5; this is mainly due to the characteristics of the Euler transform when it behaves at its best for alternating power series, which is the case of the hyperbolic NILT method. Furthermore, a precise quantitative conclusion of the accuracy of the hyperbolic NILT method with the adapted acceleration techniques can be observed by introducing the accuracy measure ξ, while considering a number of 200 points, namely

$$\xi = \sqrt{\frac{\sum_{i=1}^{200} [f(t_i) - \hat{f}(t_i)]^2}{200}} \; , \tag{2.26}$$

where $f(t_i)$ is the pre-known original and $\hat{f}(t_i)$ is the result of the hyperbolic NILT inversion. The results are shown in Tab. 2.2 for each of the acceleration techniques.
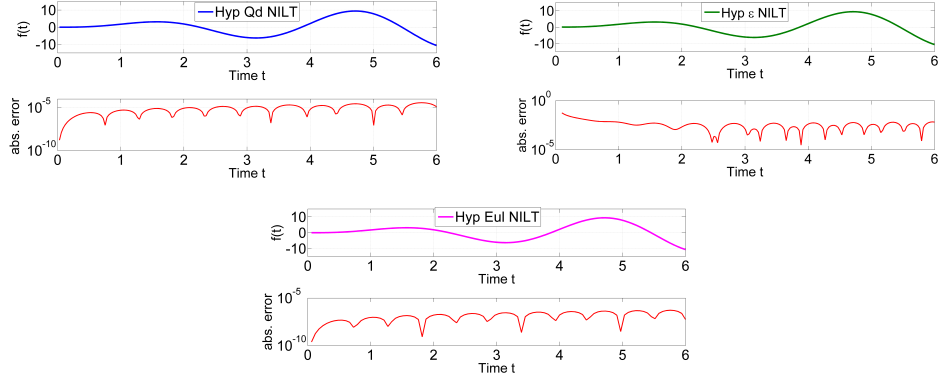
Fig. 2.3: Accuracy experiment results of the accelerated hyperbolic NILTs with test function F_1.
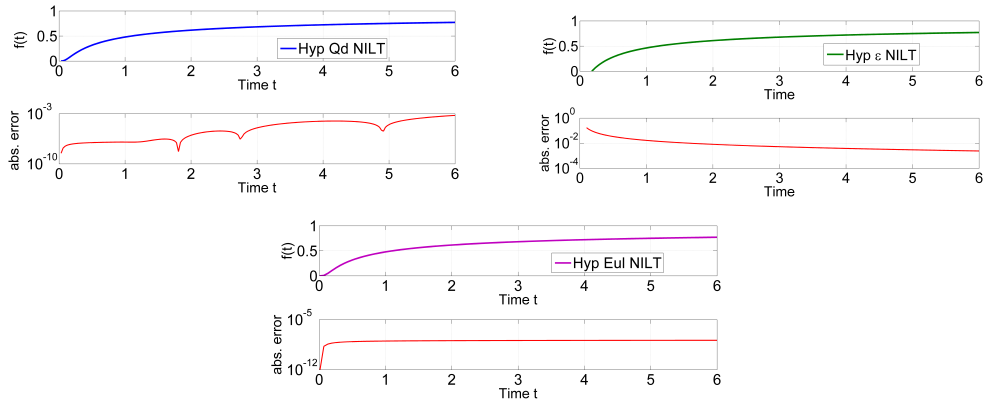

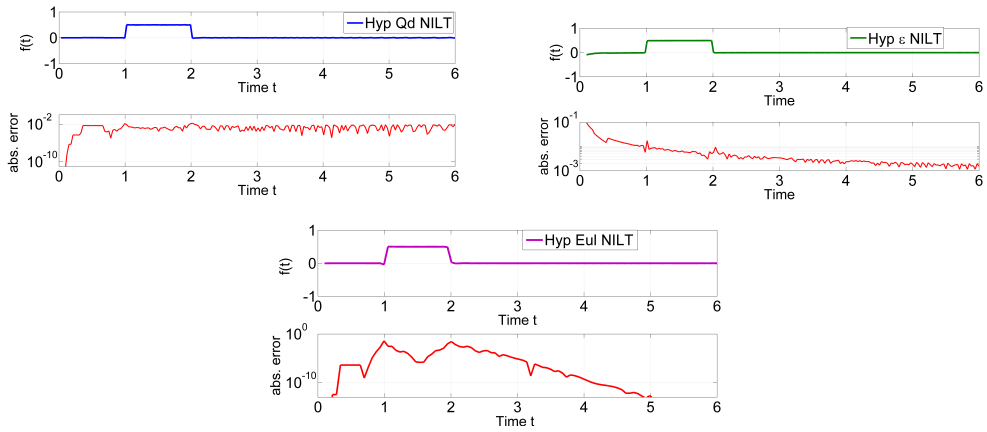Fig. 2.4: Accuracy experiment results of the accelerated hyperbolic NILTs with test function F_2.

Fig. 2.5: Accuracy experiment results of the accelerated hyperbolic NILTs with test function F_3.

Tab. 2.2: 1D hyperbolic NILT ξ accuracy measures.

F_r	Hyp-ε NILT	Hyp-Qd NILT	Hyp-Eul NILT
1	0.8×10^{-2}	1.34×10^{-5}	2.25×10^{-7}
2	2.3×10^{-2}	1.42×10^{-4}	1.18×10^{-8}
3	1.2×10^{-2}	7.9×10^{-2}	4.9×10^{-3}

2.2 Comparative study for the 1D hyperbolic NILT method

The 1D NILT methods analyzed in this section include:
- The Zakian 1D method [27],
- the Talbot 1D method [28],
- the Stehfest method [29],
- the 1D accelerated FFT-based method (FFT-Qd NILT) [30], and
- the NILT method based on inverse Laplace transform kernel hyperbolic approximations (Hyp-Eul NILT), [1, 5, 18, 24].

These methods were implemented by using the Matlab mathematical language and were verified as for their accuracy, stability, range of application as well as their computational speed. The methods were verified by using test functions in the Laplace domain with their pre-known originals. Tab. 2.3 shows the functions and their known originals respectively [18]. The methods were implemented by using the Matlab mathematical language and verified as for their accuracy, stability, range of application as well as their computational speed.

Tab. 2.3: List of test functions and their original-time domain values for the comparative study

r	Functions in the Laplace domain $F_r(s)$	Functions in the time domain $f_r(t)$
1	$F_1(s) = \frac{\omega}{s^2 + \omega^2}$	$f_1(t) = \sin(\omega t)$
2	$F_2(s) = \frac{e^{-a\sqrt{s}}}{\sqrt{s}}$	$f_2(t) = \frac{1}{\sqrt{\pi t}} \cdot e^{\frac{-a^2}{4t}}$
3	$F_3(s) = \frac{1}{s} \cdot \frac{1}{\exp(s) - 1}$	Staircase Function.

The results of inverting the test functions on each of the described 1D NILT methods are displayed in Fig. 2.6 to Fig. 2.8; each method was tested independently on the time interval $t = (0, 9)$ sec, [18]. The results show that for the chosen test functions, the Zakian method generally lacks accuracy for the exponential and for the staircase function; as for the sinusoidal function $f_1(t)$, the Zakian method is inverted correctly for about six oscillations and then is slowly damped. The Talbot method is more accurate on the whole-time interval, except for the staircase function, the function has jump discontinuities, and the Gibbs effect is easily noticed, as is the case with function $f_3(t)$.
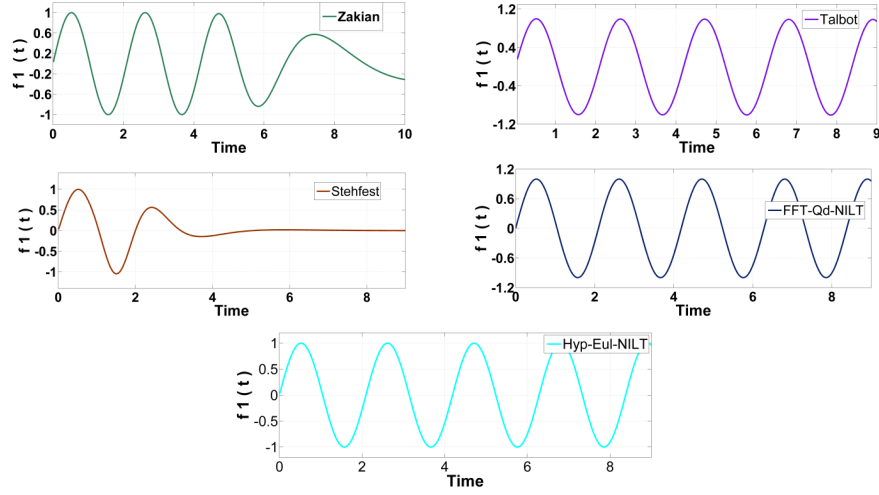
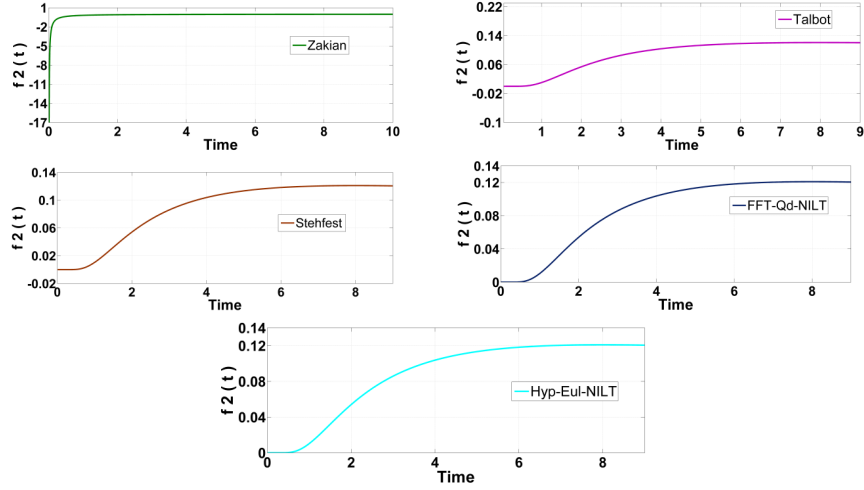Fig. 2.6: Test results of the Zakian, Talbot, Stehfest, FFT-Qd NILT and Hyp-Eul NILT methods with function F_1.

Fig. 2.7: Test results of the Zakian, Talbot, Stehfest, FFT-Qd NILT and Hyp-Eul NILT methods with function F_2.

The simulation results of the Stehfest NILT method are programmed in the Matlab language. The inversion is relatively good for the exponential function $f_2(t)$, although the results of the other two functions, $f_1(t)$ and $f_3(t)$ are not possible to be considered for practical uses due to the lack of accuracy [18]. Nevertheless, the method showed positive results in other types of functions in other fields of applications, such as the solute transport or the applications in the petrol engineering field [31]. Regarding the performed tests using the FFT-Qd NILT and the Hyp-Eul NILT, as can be noticed, their results exhibit a high accuracy and stability on the whole time interval for all the tested functions. The staircase function is an important case to look at as, due to its several discontinuities, it is usually difficult to invert such functions, but both the FFT-Qd NILT and the Hyp-Eul-NILT provide very accurate inversions for it. The Hyperbolic NILT accuracy measurement, incorporated with different accelerating techniques, has been performed by the experimental error analysis and the results have been published in [1, 24, 26]. From the error analysis performed the accuracy of the Hyp-Eul NILT is shown to be relatively very high, for instance the absolute error of the Hyp-Eul NILT inversion for the function $f(t) = \cos(\omega t)$ is bellow 10^{-10} on the time interval $t = (0, 8)$ sec.
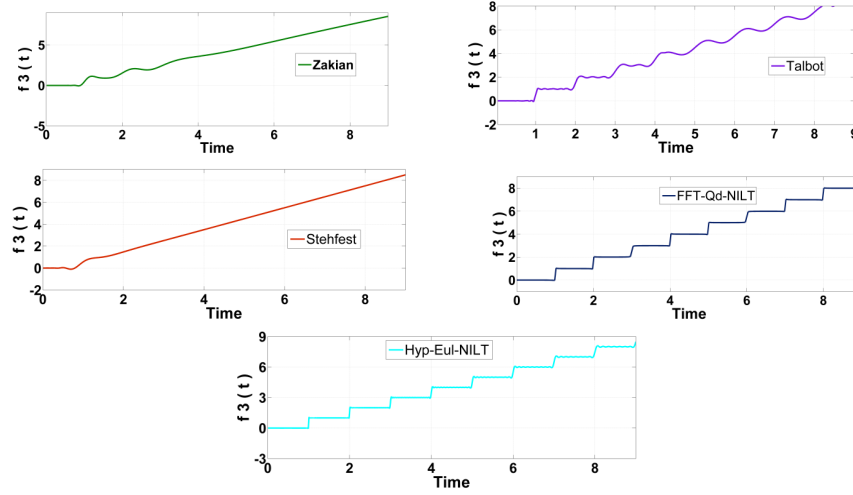
Fig. 2.8: Test results of the Zakian, Talbot, Stehfest, FFT-Qd NILT and Hyp-Eul NILT methods with function F_3.

3 APPLICATIONS OF THE 1D HYPERBOLIC NILT METHOD

In this chapter, several applications using the 1D hyperbolic NILT method, among others, are successfully implemented. These applications are focused on the simulation of voltage/current waveforms along lossy transmission lines (TL), frequency dependent TL, multiconductor TL (MTL), and including fractional-order elements in the modeling of these applications. Results of each of these applications are programmed in Matlab and illustrated in respective figures.

3.1 Lossy transmission line simulation using the hyperbolic NILT method

The NILT's field of applications are, mainly, used to process Laplace transforms that arise from the solution of systems with distributed parameters, in which their mathematical structures result in transcendental and/or irrational Laplace transforms. A practical application of the proposed 1D hyperbolic NILT method is here presented; this application involves the solution of a lossy TL and a simulation the conditions of the voltage/current waveforms along the TL wires. The TL model in the Laplace domain is shown in Fig. 3.1 bellow [18]. The Laplace model of the
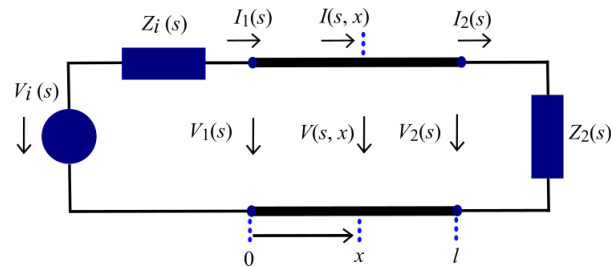

Fig. 3.1: Transmission line model in the Laplace domain.

transmission line results from the application of the Laplace transform of one variable (the time

t) on the pair of telegrapher equations

$$-\frac{\partial v(t,x)}{\partial x} = R_0 i(t,x) + L_0 \frac{\partial i(t,x)}{\partial t} \ , \tag{3.1}$$

$$-\frac{\partial i(t,x)}{\partial x} = G_0 v(t,x) + C_0 \frac{\partial v(t,x)}{\partial t} \ , \tag{3.2}$$

where R_0, L_0, G_0 and C_0 are per–unit–length (p.u.l.) elements and represent resistance, inductance, conductance and capacitance, respectively.

The Laplace transform of the solution with considering zero initial conditions, i.e. $v(0,x) = 0$ and $i(0,x) = 0$, and by incorporating boundary conditions then we get [1],

$$V(s,x) = V_i(s)\frac{Z_c(s)}{Z_i(s) + Z_c(s)} \cdot \frac{\mathrm{e}^{-\gamma(s)x} + \rho_2(s)\mathrm{e}^{-\gamma(s)[2l-x]}}{1 - \rho_1(s)\rho_2(s)\mathrm{e}^{-2\gamma(s)l}} \ , \tag{3.3}$$

$$I(s,x) = V_i(s)\frac{1}{Z_i(s) + Z_c(s)} \cdot \frac{\mathrm{e}^{-\gamma(s)x} - \rho_2(s)\mathrm{e}^{-\gamma(s)[2l-x]}}{1 - \rho_1(s)\rho_2(s)\mathrm{e}^{-2\gamma(s)l}} \ , \tag{3.4}$$

where $Z_c(s)$ and $\gamma(s)$ represent the characteristic impedance and the propagation constant of the line, respectively, and are given as

$$Z_c(s) = \sqrt{\frac{Z_0(s)}{Y_0(s)}} = \sqrt{\frac{R_0 + sL_0}{G_0 + sC_0}} \ , \tag{3.5}$$

$$\gamma(s) = \sqrt{Z_0(s) \cdot Y_0(s)} = \sqrt{(R_0 + sL_0)(G_0 + sC_0)} \ , \tag{3.6}$$

where $Z_0(s) = R_0 + sL_0$ and $Y_0(s) = G_0 + sC_0$ are p.u.l. series impedance and shunt admittance, respectively. The reflection coefficients at the beginning and end of the TL $\rho_1(s)$ and $\rho_2(s)$ accordingly, are

$$\rho_1(s) = \frac{Z_i(s) - Z_c(s)}{Z_i(s) + Z_c(s)}; \quad \rho_2(s) = \frac{Z_2(s) - Z_c(s)}{Z_2(s) + Z_c(s)} \ . \tag{3.7}$$

In this test, the simulation of a uniform transmission line with length l is performed and the following parameters are considered; $l = 2$ m, $R_0 = 10$ mΩ/m, $L_0 = 227$ nH/m, $G_0 = 2$ mS/m, $C_0 = 90.9$ pF/m, $Z_i = 30$ Ω, $Z_2 = 3$ kΩ. The transmission line is tested with an excitation wave $v_i(t) = \sin^2\left(\frac{\pi t}{4 \cdot 10^{-9}}\right)$ with $0 \le t \le 4 \cdot 10^{-9}$, and $v_i(t) = 0$, otherwise. The corresponding Laplace domain of the excitation voltage waveform is $V_i(s) = \frac{2\pi^2[1 - \exp(-4 \cdot 10^{-9}s)]}{s[(4 \cdot 10^{-9}s)^2 + 4 \cdot \pi^2]}$.
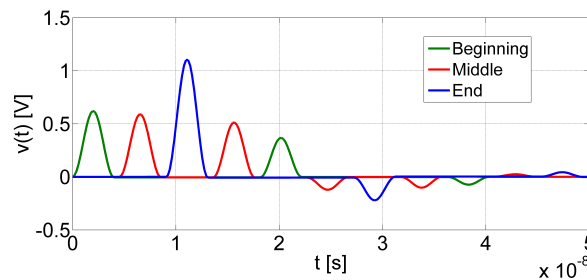

Fig. 3.2: Voltage waveforms conditions along TL by via 1D Hyp-Eul NILT.

The time-domain conditions of the voltage, and current waveforms ore obtained by using the hyperbolic 1D NILT method, the results are depicted in Fig. 3.2 and Fig. 3.3 for the beginning, middle and end of the transmission line [18].
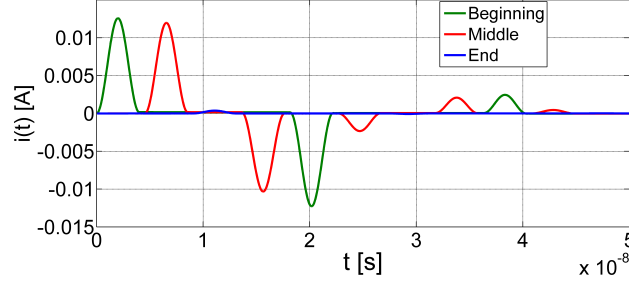
Fig. 3.3: Current waveforms conditions along TL via 1D Hyp-Eul NILT.

The parameters used for the Hyp-Eul NILT to obtain the results are: $n_{sum} = 200$, $n_{euler} = 100$ and $m \cdot a = 9$.

3.2 Incorporation of fractional-order transmission line primary parameters

Research of fractional-order calculus was introduced more than 300 years ago, with a vast field of applications benefiting from the introduction of fractional-order calculus, and still many potential topics in this field that are open for further research and discussion [32–34]. Due to the advantage of having the NILT methods in hand, it is thus possible to introduce the fractional-order domain of different application models in the Laplace domain and thus highly simplifying the solution process.

In the following subsections, we introduce the fractional-order primary parameters to the TL mode, with detailed analysis being performed. Following, the fractional-order TL resulting model is tested via an excitation waveform, and with the assistance of the Hyp-Qd NILT, we can simulate the voltage/current waveforms along the TL in the time-domain.

I. Fractional-order primary parameters

Considering a TL of length l with distributed elements, as in Fig. 3.1, the TL has the elementary section shown in Fig. 3.4. The primary parameters L'_0, C'_0 have the fractional orders α and β, respectively, where the dash designation represents only the fractional order immittances, keeping into account the numerical value of parameters is unchanged. As it

Fig. 3.4: Fractional-order primary parameters of the TL.
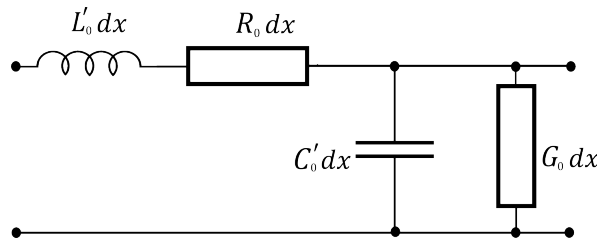
will be demonstrated, imposing fractional parameters give a higher degree of freedom for TL modeling and optimization, enabling the realization of the losses, especially those resulting from high frequencies [35], and furthermore building on the fact that the solution of the TL traveling waveforms continuously depends on the fractional derivative. Incorporating the

17

fractional-order primary parameters into transmission line systems of equations results in

$$Z_{cf} = \sqrt{\frac{Z_{0f}(s)}{Y_{0f}(s)}} = \sqrt{\frac{R_0 + s^{\alpha} L_0'}{G_0 + s^{\beta} C_0'}} \ , \tag{3.8}$$

where $Z_{cf}(s)$ annotates the fractional-order characteristic impedance, which is replaced instead of the integer-order characteristic impedance $Z_c(s)$ in (3.5). Consequently, the propagation constant $\gamma(s)$ changes accordingly with fractional parameters as

$$\gamma_f(s) = \sqrt{Z_{0f}(s) \cdot Y_{0f}(s)} = \sqrt{(R_0 + s^{\alpha} L_0')(G_0 + s^{\beta} C_0')} \ . \tag{3.9}$$

II. Fractional-order model analysis and results

R. Ismail et al. [36], discuss the effects of the fractional parameters α and β on the real part of the propagation constant (the attenuation) and the real part of the characteristic impedance (the resistive element). Moreover, in the recent work in [37], we argue that by checking the sign of the real part of the propagation constant γ, which should remain negative as it represents attenuation and in practice $0 < \alpha, \beta < 2$, then the region of the fractional parameters α and β are found to be in the range $1 < \alpha + \beta < 3$; illustrations of this study are shown in Fig. 3.5, [37]. Furthermore, it is interesting to notice, when analyzing the fractional-order characteristic impedance, that the real part of Z_{cf}, which represents the resistive element, is affected by the fractional parameters α and β. Mainly, with a constant load, the TL response to applied voltage is resistive rather than reactive, despite being composed of inductive, capacitive and resistive elements. The integer-model case of characteristic impedance can be noticed in the Fig. 3.6 (a) and that is when $\alpha = 1$ and $\beta = 1$. Interestingly, the real value of the characteristic impedance (resistive element) is positive and increasing when the fractional values are in the range $0 < \alpha, \beta < 1$ and hence we bound our choices in this region; above this range the real value of the characteristic impedance is negative and decreasing as shown in Fig. 3.6 (c).

The relation of $Z_{cf}(s)$ and $\gamma_f(s)$ with the fractional parameters α and β are shown in Fig. 3.5 and Fig. 3.6, accordingly. The sub-figures (a), (b) and (c) illustrate the real value with the regions of interest which bound the selection of α, β. The simulations are done in Matlab with $s = j\omega$, where ω is the angular frequency and is chosen as $\omega = 1 \times 10^9 \ \mathrm{rad \cdot s^{-1}}$.
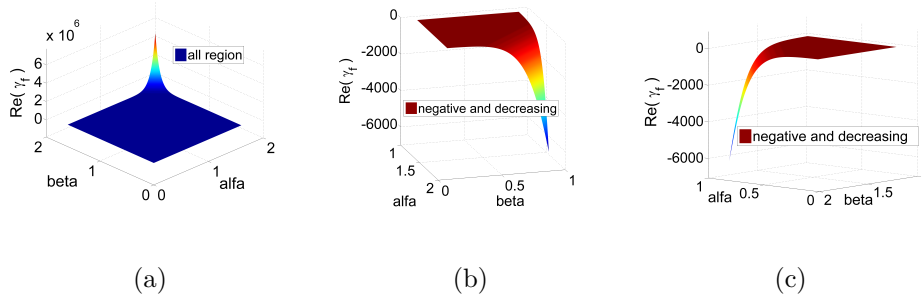

(a)   (b)   (c)

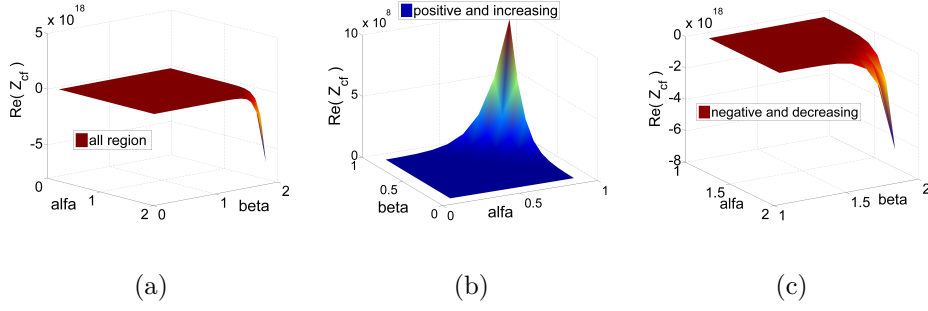Fig. 3.5: Real value of γ_f versus α and β.

Fig. 3.6: Real value of Z_{cf} versus α and β.

3.3 Incorporation of frequency dependent transmission line parameters

Due to continuous rapid increase in operational frequencies and transmission speeds in power systems, an essential characteristic to be considered is the frequency dependence properties. Generally, skin effect (SE) is an important frequency dependent parameter to be considered when dealing with high frequency applications [38]; its impact is usually higher than the polarization effect on the surrounding medium [39]. Mainly, skin effect increases the resultant losses of the TL. By transforming the skin effect into the Laplace-domain the solution is effectively simplified, rather than solving in the time-domain. The fractional-order series impedance is supplemented by the term $K\sqrt{s}$, to give

$$Z_{0f}(s) = R_0 + s^\alpha L_0' + K\sqrt{s} \ , \tag{3.10}$$

where the added rightmost term represents both high-frequency internal resistance and internal inductive reactance. Skin effect can be described as the tendency of a high-frequency electric current to distribute itself in a conductor so that the current density near the surface is greater than at its core. The transmission line parameters have obvious frequency-dependent phenomena due to the skin and edge effect on high frequencies. Taking into account the SE and other conditions, the calculation and analysis of frequency-dependent transmission line gives more accurate transmission characteristics. Therefore, (3.10) will be used in (3.8) and (3.9) in the following analysis.

3.4 Fractional-order TL model simulation

For this study, let us consider a lossy transmission line of length $l = 2$ m, $R_0 = 0.35$ Ω/m, $L_0 = 265$ nH/m, $G_0 = 0.1$ mS/m, $C_0 = 95$ pF/m, $Z_i = 10$ Ω, $Z_2 = 2.5$ kΩ, and the skin effect parameter $K = 4.5 \cdot 10^{-4}$ $\Omega\sqrt{s}$/m for frequency dependent line or $K = 0$ is used for the frequency independent line [40], and with the fractional parameters α and β used for the inductance and capacitance, accordingly. The fractional-order characteristic impedance with incorporating the skin effect is given as

$$Z_{cf} = \sqrt{\frac{R_0 + s^\alpha L_0' + K\sqrt{s}}{G_0 + s^\beta C_0'}} \ . \tag{3.11}$$

Consequently, the fractional-order propagation constant with the skin effect is given as

$$\gamma_f(s) = \sqrt{(R_0 + s^\alpha L_0' + K\sqrt{s})(G_0 + s^\beta C_0')} \ . \tag{3.12}$$

After substituting the characteristic impedance and the propagation constant, in their fractional-order form, into (3.3) and (3.4), then the voltage/current waveforms are effectively obtained in the time-domain by undergoing the proposed hyperbolic numerical inverse Laplace transform (Hyp-

Qd NILT) method, accelerated with the quotient-difference algorithm. For this analysis the TL was excited with the voltage waveform [37]

$$v_i(t) = \begin{cases} \sin^2\left(\frac{\pi \cdot t}{2 \cdot 10^{-9}}\right), & \text{for } 0 < t < 2 \cdot 10^{-9} \\ 0, & \text{elsewhere}. \end{cases},$$

The excitation waveform is first converted to the Laplace domain i.e:

$$V_i(s) = \frac{2\pi^2(1 - \exp(-2 \cdot 10^9 s))}{s((2 \cdot 10^{-9}s)^2 + 4\pi^2)},$$

and then the voltage/current waveforms are simulated for three cases; the integer TL model, the integer TL model with frequency dependence parameters and the fractional-order TL model with frequency dependent parameters; results are illustrated in Fig. 3.7 and Fig. 3.8 for voltage and current waveforms, respectively. By observing these and comparing the fractional-order model including skin effect with the integer-model, it is noticed that the results capture more realistically the TL properties which are neglected in the integer model.
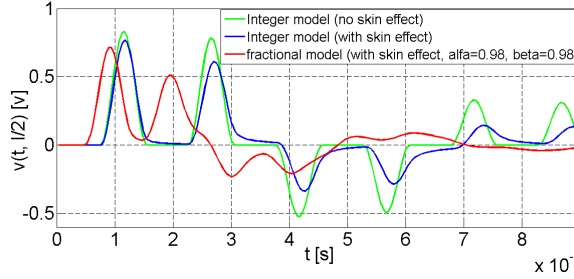

Fig. 3.7: Voltage waveform in the middle of the TL ($x = 1\,\text{m}$).
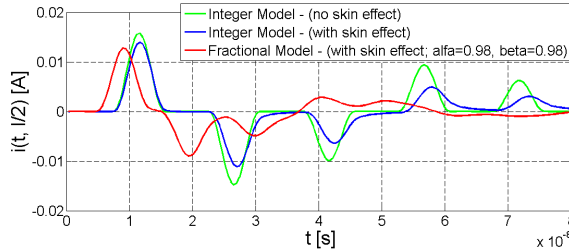

Fig. 3.8: Current waveform in the middle of the TL ($x = 1\,\text{m}$).

In Fig. 3.9 and Fig. 3.10 are illustrated the voltage distributions, along the same TL example described above, with the choices of fractional parameters $\alpha, \beta = 0.98$ in Fig. 3.9, and $\alpha, \beta = 0.95$ in Fig. 3.10; these values are selected to be in the range bounded by checking the sing of the real value of Z_{cf} and γ_f. It is evident that when $\alpha, \beta = 0.95$ the diffusion is faster than when $\alpha, \beta = 0.98$, [37]. These results are consistent with the behavior of fractional order systems. In essence, as the forward wave and reflected wave travel in opposite directions, this leads to a change in the traveling wave shape and range. As a result, the fractional transmission line model captures the abnormal diffusion phenomena of the voltage wave in the TL much more precisely than the classical integer mode. The simulation results shown in Fig. 3.7 and Fig. 3.8 were computed using the 1D hyperbolic NILT method accelerated with the QdA, on the other hand the 3D voltage and current distributions in Fig. 3.9 and Fig. 3.10, respectively, were obtained by the 2D FFT-NILT method.
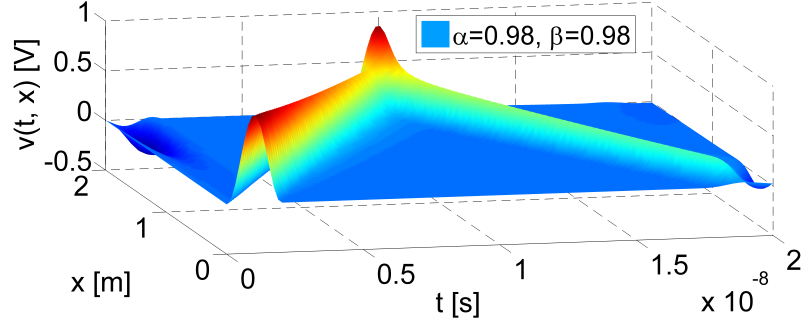
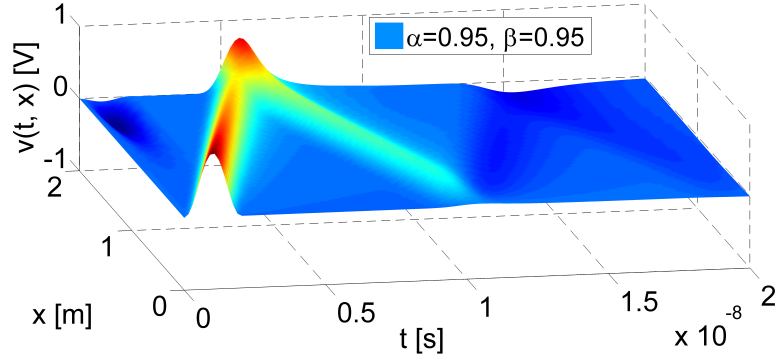Fig. 3.9: Voltage distribution along the TL with fractional-order parameters ($\alpha = \beta = 0.98$).

Fig. 3.10: Voltage distribution along the TL with fractional-order parameters ($\alpha = \beta = 0.95$).

3.5 Multiconductor transmission line systems with linear terminations

Multiconductor transmission lines (MTLs) are often found in communication systems, power distribution systems, and digital computers, [41]. Thus, the analysis of such systems comes out to be of high practical importance. In the previous sections, we examined the time-domain analysis of the TL system equations and incorporated frequency dependences, nonuniformity, and fractional-order elements. In this section, we will focus on MTLs, which consist of more than two conductors, with linear terminations. It will be shown that the process to expand the result obtained for the TL to the MTL is straightforward, mainly done by introducing the matrix notation. Generally, there are many methods that can be considered when simulating MTL, such as the derivation of the MTL equations from the integral form of Maxwell's equations, derivation of the MTL equations from the p.u.l. equivalent circuit, utilizing the 'implicit Wendroff and state variable' method and others, [39, 42, 43]. Nevertheless, by the advantage of using NILT method, the analysis of MTLs can be done much more time effectively and enable us to introduce all different losses and effects on the modeling, including fractional-order elements, in a simple and fast manner.

This section will be dedicated to an advanced solution of MTLs terminated on both ends with linear networks; these terminations can be modeled by generalized Thevénin and/or Norton equivalents. In the next section MTLs with more complex terminations and possible external feedbacks, describable with a modified nodal analysis and utilizing the NILT method, will be addressed. In this analysis, we will consider a MTL system containing an $(n + 1)$-conductor TL with length l for each of the lines, which has the p.u.l. $n \times n$ matrices $\mathbf{R}$, $\mathbf{L}$, $\mathbf{G}$, and $\mathbf{C}$; noting
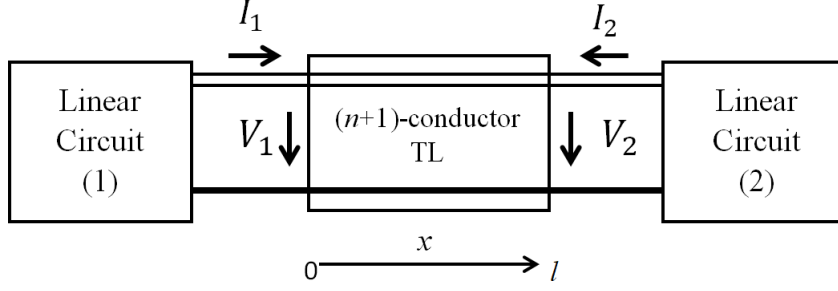
Fig. 3.11: General $(n + 1)$-conductor TL system with linear terminations.

that the bold symbols here represent matrices, in contrast to the normal parameters used for a single TL in previous sections, [41].

Firstly, let us start with the description of a classical MTL, afterwards fractional-order elements will be incorporated. A uniform $(n + 1)$-conductor TL can be presented by a pair of telegraph equations in the time domain with assuming zero initial conditions, i.e. $\mathbf{v}(0, x) = 0$ and $\mathbf{i}(0, x) = 0$.

$$-\frac{\partial \mathbf{v}(t, x)}{\partial x} = \mathbf{R}\mathbf{i}(t, x) + \mathbf{L}\frac{\partial \mathbf{i}(t, x)}{\partial t} \ , \tag{3.13}$$

$$-\frac{\partial \mathbf{i}(t, x)}{\partial x} = \mathbf{G}\mathbf{v}(t, x) + \mathbf{C}\frac{\partial \mathbf{v}(t, x)}{\partial t} \ , \tag{3.14}$$

where $\mathbf{v}(t, x)$ and $\mathbf{i}(t, x)$ are $n \times 1$ column vectors of the voltages and currents of n active wires at the distance x from the MTL's left side, accordingly. For simplicity purposes, we can represent the above telegraph equations (3.13) and (3.14) in a compact matrix form

$$\frac{\partial}{\partial x}\begin{bmatrix} \mathbf{v}(t, x) \\ \mathbf{i}(t, x) \end{bmatrix} = \begin{bmatrix} \mathbf{0} & -\mathbf{R} \\ -\mathbf{G} & \mathbf{0} \end{bmatrix} \cdot \begin{bmatrix} \mathbf{v}(t, x) \\ \mathbf{i}(t, x) \end{bmatrix} - \begin{bmatrix} \mathbf{0} & \mathbf{L} \\ \mathbf{C} & \mathbf{0} \end{bmatrix} \cdot \frac{\partial}{\partial t}\begin{bmatrix} \mathbf{v}(t, x) \\ \mathbf{i}(t, x) \end{bmatrix} , \tag{3.15}$$

transforming (3.15) into the Laplace domain with respect to the time variable t

$$\frac{d}{dx}\begin{bmatrix} \mathbf{V}(s, x) \\ \mathbf{I}(s, x) \end{bmatrix} = \begin{bmatrix} \mathbf{0} & -\mathbf{Z}(s) \\ -\mathbf{Y}(s) & \mathbf{0} \end{bmatrix} \cdot \begin{bmatrix} \mathbf{V}(s, x) \\ \mathbf{I}(s, x) \end{bmatrix} , \tag{3.16}$$

where the $n \times 1$ voltage and current vectors $\mathbf{V}(s, x) = \mathbf{L}\{\mathbf{v}(t, x)\}$ and $\mathbf{I}(s, x) = \mathbf{L}\{\mathbf{i}(t, x)\}$, respectively. The matrix $\mathbf{0}$ stands for the $n \times n$ order zero matrix, and the series impedance matrix and shunt admittance matrix are given, respectively, as follows

$$\mathbf{Z}(s) = \mathbf{R} + s\mathbf{L} \ , \tag{3.17}$$

$$\mathbf{Y}(s) = \mathbf{G} + s\mathbf{C} \ . \tag{3.18}$$

When considering the boundary condition at $x = 0$, $\mathbf{V}_1(s) = \mathbf{V}(s, 0)$ and $\mathbf{I}_1(s) = \mathbf{I}(s, 0)$, see Fig. 3.11, a formal solution is

$$\begin{bmatrix} \mathbf{V}(s, x) \\ \mathbf{I}(s, x) \end{bmatrix} = \exp\left(\begin{bmatrix} \mathbf{0} & -\mathbf{Z}(s) \\ -\mathbf{Y}(s) & \mathbf{0} \end{bmatrix} \cdot x\right) \cdot \begin{bmatrix} \mathbf{V}_1(s) \\ \mathbf{I}_1(s) \end{bmatrix} . \tag{3.19}$$

If the MTL is considered as a multiport then the matrix exponential function (3.19) can be considered as a chain matrix

$$\mathbf{\Phi}(s, x) = \begin{bmatrix} \mathbf{\Phi}_{11}(s, x) & \mathbf{\Phi}_{12}(s, x) \\ \mathbf{\Phi}_{21}(s, x) & \mathbf{\Phi}_{22}(s, x) \end{bmatrix} = \exp\left(\begin{bmatrix} \mathbf{0} & -\mathbf{Z}(s) \\ -\mathbf{Y}(s) & \mathbf{0} \end{bmatrix} \cdot x\right) , \tag{3.20}$$

where $\mathbf{\Phi}_{ij}(s,x)$, $i,j = 1,2$, are respective $n \times n$ square submatrices. noting that due to the MTL reciprocity, $\det(\mathbf{\Phi}(s)) = 1$, though, in general $\mathbf{\Phi}_{11}(s) \neq \mathbf{\Phi}_{22}(s)$ due to some possible inhomogeneity. Now, for simplicity, let us designate the chain matrix of the whole MTL of the length l as $\mathbf{\Phi}(s,l) = \mathbf{\Phi}(s)$. Then, by using e.g. a generalized Thévenin equivalents of both terminating linear circuits the formulae for the boundary vectors $\mathbf{I}_1(s)$ and $\mathbf{V}_1(s)$ can be determined as

$$\begin{aligned} \mathbf{I}_1(s) = &[(\mathbf{\Phi}_{11}(s) - \mathbf{Z}_{i2}(s)\mathbf{\Phi}_{21}(s))\mathbf{Z}_{i1}(s) + \mathbf{Z}_{i2}(s)\mathbf{\Phi}_{22}(s) - \mathbf{\Phi}_{12}(s)]^{-1} \times \\ &[(\mathbf{\Phi}_{11}(s) - \mathbf{Z}_{i2}(s)\mathbf{\Phi}_{21}(s))\mathbf{V}_{i1}(s) - \mathbf{V}_{i2}(s)] \end{aligned} \quad , \quad (3.21)$$

$$\mathbf{V}_1(s) = \mathbf{V}_{i1}(s) - \mathbf{Z}_{i1}(s)\mathbf{I}_1(s) \ , \quad (3.22)$$

where $\mathbf{V}_{i1}(s)$, $\mathbf{V}_{i2}(s)$, and $\mathbf{Z}_{i1}(s)$, $\mathbf{Z}_{i2}(s)$ are internal voltage vectors and internal impedance matrices of the respective Thévenin equivalents, respectively. Nevertheless, other combinations of Thévenin and/or Norton equivalents can be considered for both ends of the MTL, namely, Norton left side $\rightarrow$ Norton right side:

$$\begin{aligned} \mathbf{V}_1(s) = &[(\mathbf{\Phi}_{22}(s) - \mathbf{Y}_{i2}(s)\mathbf{\Phi}_{12}(s))\mathbf{Y}_{i1}(s) + \mathbf{Y}_{i2}(s)\mathbf{\Phi}_{11}(s) - \mathbf{\Phi}_{21}(s)]^{-1} \times \\ &[(\mathbf{\Phi}_{22}(s) - \mathbf{Y}_{i2}(s)\mathbf{\Phi}_{12}(s))\mathbf{I}_{i1}(s) + \mathbf{I}_{i2}(s)] \ , \end{aligned} \quad (3.23)$$

Thévenin left side $\rightarrow$ Norton right side:

$$\begin{aligned} \mathbf{I}_1(s) = &[(\mathbf{\Phi}_{21}(s) - \mathbf{Y}_{i2}(s)\mathbf{\Phi}_{11}(s))\mathbf{Z}_{i1}(s) + \mathbf{Y}_{i2}(s)\mathbf{\Phi}_{12}(s) - \mathbf{\Phi}_{22}(s)]^{-1} \times \\ &[(\mathbf{\Phi}_{21}(s) - \mathbf{Y}_{i2}(s)\mathbf{\Phi}_{11}(s))\mathbf{V}_{i1}(s) + \mathbf{I}_{i2}(s)] \end{aligned} \quad , \quad (3.24)$$

Norton left side $\rightarrow$ Thévenin right side:

$$\begin{aligned} \mathbf{V}_1(s) = &[(\mathbf{\Phi}_{12}(s) - \mathbf{Z}_{i2}(s)\mathbf{\Phi}_{22}(s))\mathbf{Y}_{i1}(s) + \mathbf{Z}_{i2}(s)\mathbf{\Phi}_{21}(s) - \mathbf{\Phi}_{11}(s)]^{-1} \times \\ &[(\mathbf{\Phi}_{12}(s) - \mathbf{Z}_{i2}(s)\mathbf{\Phi}_{22}(s))\mathbf{I}_{i1}(s) + \mathbf{V}_{i2}(s)] \ , \end{aligned} \quad (3.25)$$

Incorporating fractional-order elements into the MTL model is done first by interchanging the p.u.l. series impedance $\mathbf{Z}(s)$ and shunt admittance $\mathbf{Y}(s)$ matrices with $Z_f(s)$ and $\mathbf{Y}_f(s)$, respectively, as follows

$$\mathbf{Z}_f(s) = \mathbf{R} + s^\alpha \mathrm{L}_\alpha \ , \quad (3.26)$$

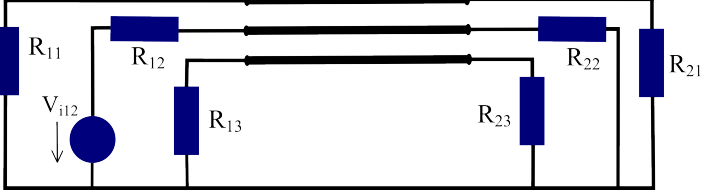$$\mathbf{Y}_f(s) = \mathbf{G} + s^\beta \mathrm{C}_\beta \ , \quad (3.27)$$

The skin effect of the MTL can be incorporated in a similar manner as done for the single TL by the modification of the series impedance (3.26) with the introduction of the term $\mathbf{K}\sqrt{s}$, though with $\mathbf{K}$ as a matrix coefficient, i.e. $\mathbf{Z}_f(s) = \mathbf{R} + s^\alpha \mathbf{L}_\alpha + \mathbf{K}\sqrt{s}$. A second simplified approach to solve the MTL system equations can be also done by performing another Laplace transform with respect to the geometric coordinate x, [44], while considering fractional-order MTL elements, which leads to the following matrix equation in the (s,q) Laplace domain,

$$\begin{pmatrix} \mathbf{V}(s,q) \\ \mathbf{I}(s,q) \end{pmatrix} = \begin{pmatrix} q\mathbf{E} & \mathbf{Z}_f(s) \\ \mathbf{Y}_f(s) & q\mathbf{E} \end{pmatrix}^{-1} \cdot \begin{pmatrix} \mathbf{V}_1(s) \\ \mathbf{I}_1(s) \end{pmatrix} , \quad (3.28)$$

where $\mathbf{E}$ is the identity matrix, and the voltage and current vectors that correspond to the left side of the MTL are obtained by computing the generalized Thévenin equivalents for both terminating linear circuits, as shown in (3.21) and (3.22), respectively. Henceforth, the time domain results can be obtained by undergoing the 2D FFT-NILT method in a fast and accurate process [45]; further details on utilizing the 2D NILT are available in the following Chapters 4 and 5.

3.5.1 Fractional-order MTL case study

A main characteristic of the proposed fractional-order MTL model and simulation is its direct support of several physical phenomena which have not been supported yet. In this case study we demonstrate the applicability of the NILT method to a practically-relevant MTL application. Let us examine a (3+1)-conductor TL, as shown if Fig. 3.12, with the length $l = 1.2$ m. The MTL has the following terminal resistors $R_{1i} = R_{2i} = 1\,\Omega$, where $i = 1, 2, 3$. The MTL's p.u.l. matrices are as follows: [46],

Fig. 3.12: A $(3 + 1)$-conductor TL system.

$$\mathbf{R} = \begin{pmatrix} 41.7 & 0 & 0 \\ 0 & 41.7 & 0 \\ 0 & 0 & 41.7 \end{pmatrix} \frac{\Omega}{\text{m}}; \quad \mathbf{L}_\alpha = \begin{pmatrix} 2.4 & 0.69 & 0.64 \\ 0.69 & 2.36 & 0.69 \\ 0.64 & 0.69 & 2.4 \end{pmatrix} \frac{\mu\text{H}}{\text{m}};$$

$$\mathbf{C}_\beta = \begin{pmatrix} 21 & -12 & -4 \\ -12 & 26 & -12 \\ -4 & -12 & 21 \end{pmatrix} \frac{\text{pF}}{\text{m}}; \quad \mathbf{G} = \begin{pmatrix} 0.6 & 0 & 0 \\ 0 & 0.6 & 0 \\ 0 & 0 & 0.6 \end{pmatrix} \frac{\text{mS}}{\text{m}}. \tag{3.29}$$

The voltage source $V_{i1,2}$ driving the second wire in Fig. 3.12 is excited by the same waveform used in Sect. 3.4. As this MTL is considered to have zero initial conditions, it is thus not required to compute matrix convolution integrals. The time-domain final results are obtained by using the 1D NILT method based on FFT accelerated with the Qd algorithm in its matrix form. The simulation results of the voltage/current propagations along the different MTL wires are illustrated in Fig. 3.13 to Fig. 3.24, where three cases are shown; namely, the classic integer case, i.e. $\alpha = \beta = 1$, fractional-order case with $\alpha = \beta = 0.97$, and the fractional-order case $\alpha = \beta = 0.87$, respectively.
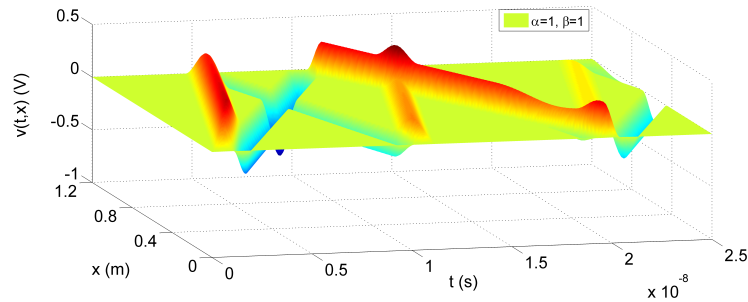

Fig. 3.13: Voltage distribution on the 1st and the 3rd line with integer-orders $\alpha = \beta = 1$.
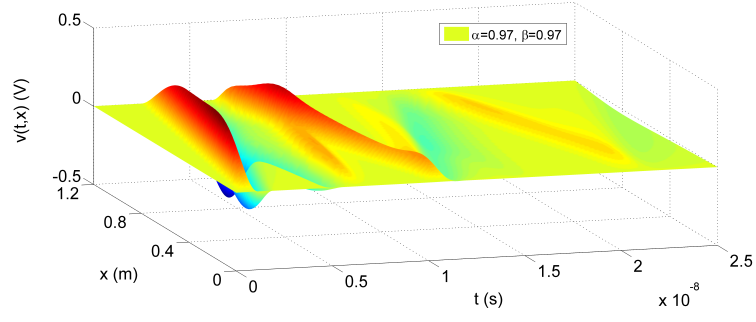
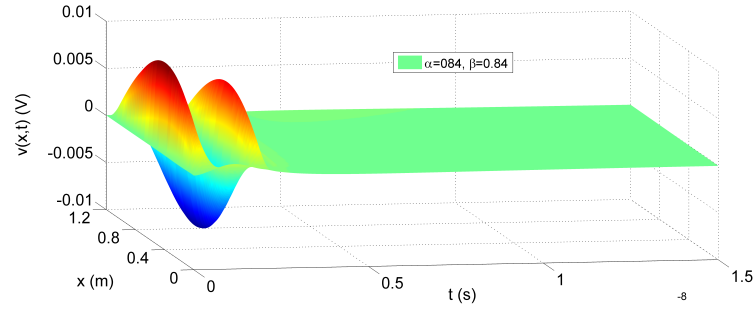Fig. 3.14: Voltage distribution on the 1ˢᵗ and the 3ʳᵈ line with fractional-orders $\alpha = \beta = 0.97$.

Fig. 3.15: Voltage distribution on the 1ˢᵗ and the 3ʳᵈ line with fractional-orders $\alpha = \beta = 0.84$.

Fig. 3.16: Current distribution on the 1ˢᵗ and the 3ʳᵈ line with integer-orders $\alpha = \beta = 1$.

Fig. 3.17: Current distribution on the 1ˢᵗ and the 3ʳᵈ line with fractional-orders $\alpha = \beta = 0.97$.

Fig. 3.18: Current distribution on the 1$^{\text{st}}$ and the 3$^{\text{rd}}$ line with fractional-orders $\alpha = \beta = 0.84$.
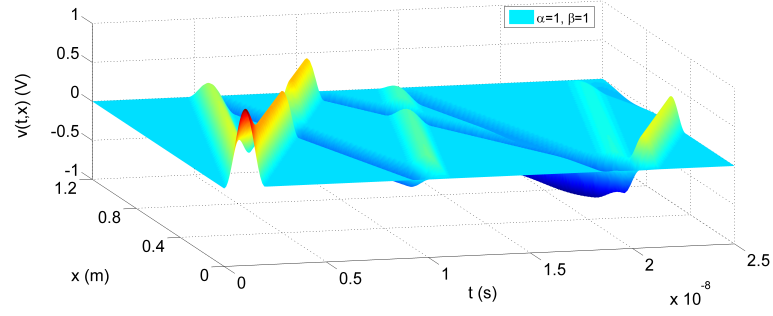
Fig. 3.19: Voltage distribution on the 2$^{\text{nd}}$ line with integer-orders $\alpha = \beta = 1$.

Fig. 3.20: Voltage distribution on the 2$^{\text{nd}}$ line with fractional-orders $\alpha = \beta = 0.97$.

Fig. 3.21: Voltage distribution on the 2$^{\text{nd}}$ line with fractional-orders $\alpha = \beta = 0.84$.
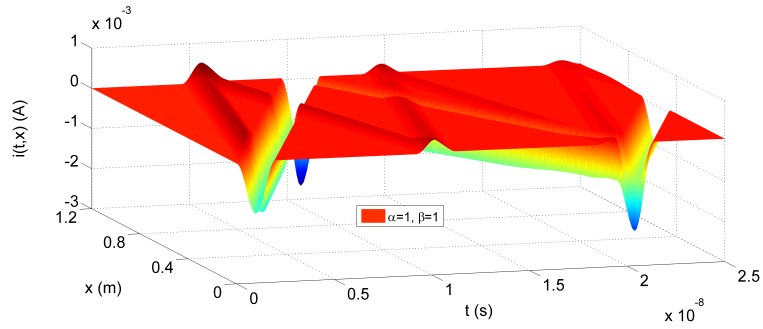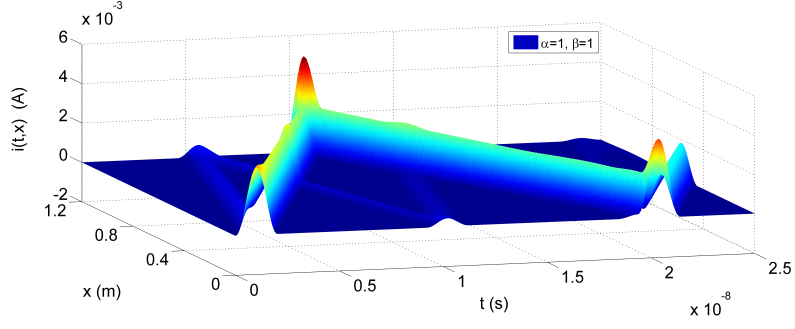
Fig. 3.22: Current distribution on the 2nd line with integer-orders $\alpha = \beta = 1$.
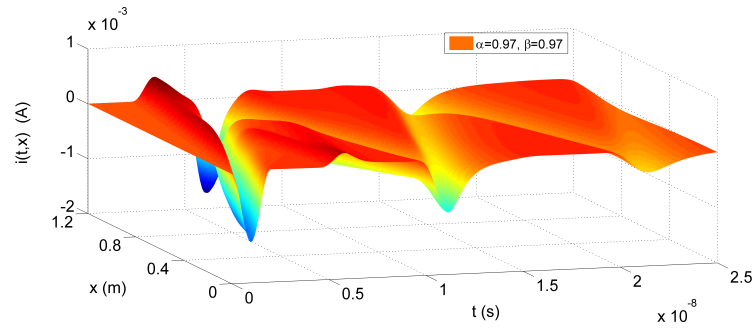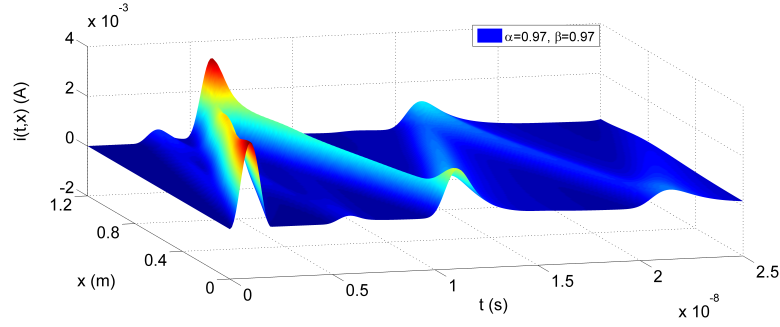

Fig. 3.23: Current distribution on the 2nd line with fractional-orders $\alpha = \beta = 0.97$.
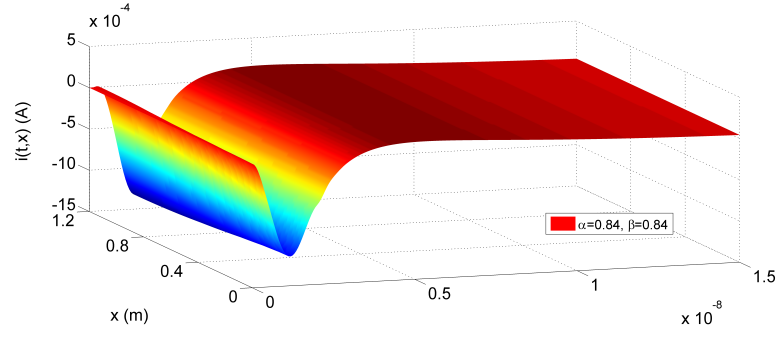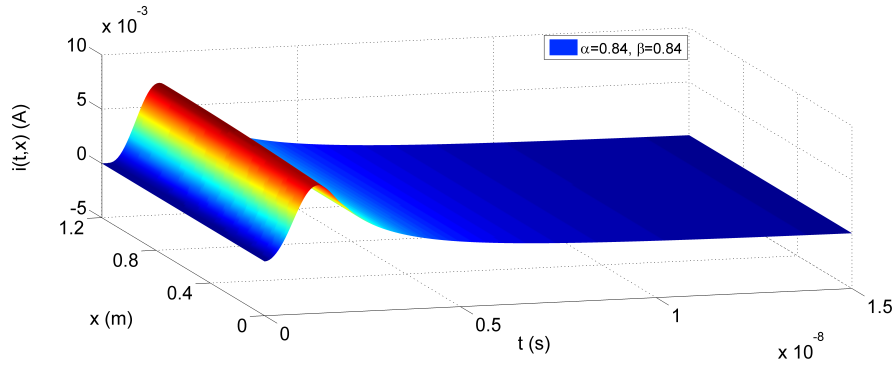

Fig. 3.24: Current distribution on the 2nd line with fractional-orders $\alpha = \beta = 0.84$.
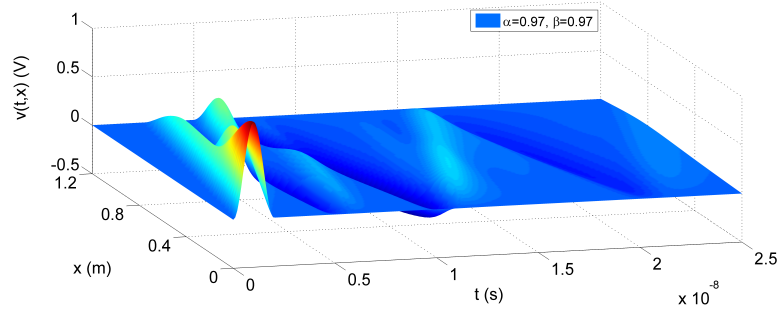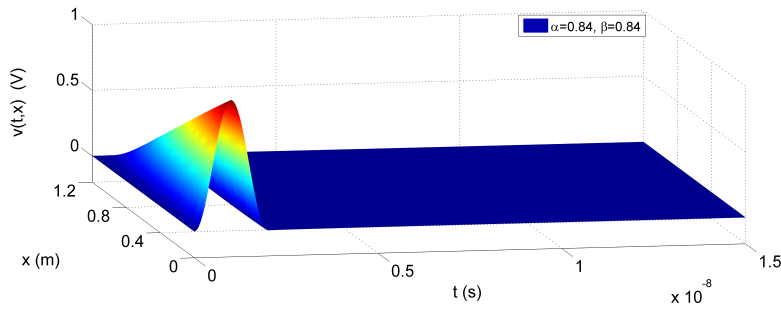
In general, Fig. 3.13 to Fig. 3.24 exhibit the voltage and current waveform distribution along the MTL wires for $\alpha, \beta = 0.84, 0.97$ and 1; while, Fig. 3.13, Fig. 3.16, Fig. 3.19, and Fig. 3.22 show the solutions of voltage/current waveforms for the classical (integer-order) MTL. Comparing the MTL simulation result figures with regard to the change in fractional-orders, we can find out that with the increase of the fractional-orders from 0.84 to 0.97, the waveform has a faster spread at the beginning; this agrees with the results of the single TL simulations obtained in Sect. 3.4, and with the diffusion theory investigated in [47, 48]. Moreover, observing the results when introducing fractional-orders, such as a comparison between Fig. 3.22 and Fig. 3.23 for the current distributions, shows that the waveform exhibits more attenuation along the wire, and hence this compensates for power losses and gives a higher degree of optimization. Looking into Fig. 3.20 and Fig. 3.21, it is noticed that the superposition effect that happens on TL wires when the forward wave and reflected wave interact is obvious in these two figures; this further shows that

the physical phenomenon of MTL is more accurately modeled using fractional-order techniques. The main advantage of utilizing the 1D FFT-NILT accelerated by the Qd algorithm [49], in its matrix form, can be seen from the obtained 3D MTL simulation results. The method allows us to solve the waves on all the MTL's wires in parallel. Depending on the defined resolution of the results and the number of terms considered for the 1D FFT-NILT computations, the average CPU time for the simulations is approximately 4 to 6 seconds running on a common PC.

In principle, the 1D FFT-NILT method is devised based on computing the inverse Laplace transform (ILT), of Bromwich definition integral, numerically on a whole given interval $(0, t_m)$. The original approach of this method was proposed in reference [49], where the FFT algorithm is applied in order to provide the solution in an accurate and fast way. Moreover, further improvements have been done on this method, such as incorporating acceleration techniques and a development into a matrix form.

4 EXPANSION OF THE HYPERBOLIC NILT METHOD INTO THE TWO-DIMENSIONAL FORM

In continuation with the achieved results of the developed hyperbolic NILT method combined the Euler transform as a convergence acceleration technique [1, 26], in this chapter the method is expanded from the 1D field to the 2D field. This grants the ability of solving applications that contain two variables, such as continuous space-time systems simultaneously.

4.1 Numerical method of the hyperbolic NILT two-dimensional expansion

In this section, the two dimensional expansion of the proposed 1D hyperbolic NILT is conducted [26], inspired by the work done in [50], followed by a detailed error analysis.

4.1.1 Theoretical concept and basic formulae

The principal formula of a two-dimensional Laplace transform of a two variable function $f(t_1, t_2)$ where $t_1, t_2 \geq 0$, is given as

$$F(s_1, s_2) = \int_0^\infty \int_0^\infty f(t_1, t_2) e^{-s_1 t_1 - s_2 t_2} dt_1 dt_2. \tag{4.1}$$

Considering the assumption $|f(t_1, t_2)| < M e^{\alpha_1 t_1 + \alpha_2 t_2}$, where M, α_1 and α_2 are positive real constants, the object function $f(t_1, t_2)$ can be given by [51]

$$f(t_1, t_2) = -\frac{1}{4\pi^2} \int_{\gamma_1 - j\infty}^{\gamma_1 + j\infty} \int_{\gamma_2 - j\infty}^{\gamma_2 + j\infty} F(s_1, s_2) e^{s_1 t_1 + s_2 t_2} ds_1 ds_2 , \tag{4.2}$$

where $s = \gamma + j\omega$. A practical technique for the evaluation of the double integral (4.2) is done by rearranging it to the forms

$$f(t_1, t_2) = \frac{1}{2\pi j} \int_{\gamma_1 - j\infty}^{\gamma_1 + j\infty} \left(\frac{1}{2\pi j} \int_{\gamma_2 - j\infty}^{\gamma_2 + j\infty} F(s_1, s_2) e^{s_2 t_2} ds_2 \right) e^{s_1 t_1} ds_1$$

$$= \frac{1}{2\pi j} \int_{\gamma_2 - j\infty}^{\gamma_2 + j\infty} \left(\frac{1}{2\pi j} \int_{\gamma_1 - j\infty}^{\gamma_1 + j\infty} F(s_1, s_2) e^{s_1 t_1} ds_1 \right) e^{s_2 t_2} ds_2 \tag{4.3}$$

and then we introduce the partial inverse Laplace transform as follows

$$L_2^{-1}\{F(s_1, s_2)\} = F_2(s_1, t_2) = \frac{1}{2\pi j} \int_{\gamma_2 - j\infty}^{\gamma_2 + j\infty} F(s_1, s_2) e^{s_2 t_2} ds_2, \tag{4.4}$$

and

$$L_1^{-1}\{F(s_1, s_2)\} = F_1(t_1, s_2) = \frac{1}{2\pi j} \int_{\gamma_1 - j\infty}^{\gamma_1 + j\infty} F(s_1, s_2) e^{s_1 t_1} ds_1, \tag{4.5}$$

consequently, the two equivalent formulae can be given as

$$f(t_1, t_2) = L_1^{-1}\{F_2(s_1, t_2)\} = \frac{1}{2\pi j} \int_{\gamma_1 - j\infty}^{\gamma_1 + j\infty} F_2(s_1, t_2) e^{s_1 t_1} ds_1$$

$$= L_2^{-1}\{F_1(t_1, s_2)\} = \frac{1}{2\pi j} \int_{\gamma_2 - j\infty}^{\gamma_2 + j\infty} F_1(t_1, s_2) e^{s_2 t_2} ds_2. \tag{4.6}$$

A symbolic expression is given as [52, 53]

$$f(t_1, t_2) = L_1^{-1}\left\{L_2^{-1}\{F(s_1, s_2)\}\right\} = L_2^{-1}\left\{L_1^{-1}\{F(s_1, s_2)\}\right\}. \tag{4.7}$$

4.1.2 The numerical method

In order to expand the hyperbolic NILT method into a 2D form, let us first start with a recapitulation of the hyperbolic relations used to approximate the exponential kernel of the i. L. t. Bromwich integral; namely, $E_{sh}(st, a) = \frac{e^a}{2\sinh(a - st)}$, $E_{ch}(st, a) = \frac{e^a}{2\cosh(a - st)}$. First we start with the $E_{ch}(st, a)$ approximation for a 2D NILT expansion, then after the first 2D NILT is devised we proceed with the second approximation i.e. the $E_{sh}(st, a)$. Henceforth, the reciprocal hyperbolic function appearing in $E_{ch}(st, a)$ is expressed by the infinite sum of rational functions

$$\frac{1}{\cosh z} = 2\pi \sum_{n=0}^{\infty} \frac{(-1)^n (n + 0.5)}{(n + 0.5)^2 \pi^2 + z^2}. \tag{4.8}$$

Replacing both exponential kernels that appear in the double integral (4.3), by their respective approximations E_{ch2} and E_{ch1}, we get

$$f_{ch}(t_1, t_2) = \frac{1}{2\pi j} \int_{\gamma_1 - j\infty}^{\gamma_1 + j\infty} \left(\frac{1}{2\pi j} \int_{\gamma_2 - j\infty}^{\gamma_2 + j\infty} F(s_1, s_2) E_{ch2} ds_2\right) E_{ch1} ds_1, \tag{4.9}$$

where the respective exponential kernels are given by

$$E_{ch2}(s_2 t_2, a) = \pi e^a \sum_{n_2 = 0}^{\infty} \frac{(-1)^{n_2}(n_2 + 0.5)}{(n_2 + 0.5)^2 \pi^2 + (a - s_2 t_2)^2}, \tag{4.10}$$

$$E_{ch1}(s_1 t_1, a) = \pi e^a \sum_{n_1 = 0}^{\infty} \frac{(-1)^{n_1}(n_1 + 0.5)}{(n_1 + 0.5)^2 \pi^2 + (a - s_1 t_1)^2}. \tag{4.11}$$

By performing the first partial i. L. t. based on (4.4) , with the intention to reach the symbolic expression (4.7), we get

$$F_{ch2}(s_1, t_2, a) = \frac{e^a}{2j} \int_{\gamma_2 - j\infty}^{\gamma_2 + j\infty} F(s_1, s_2) \sum_{n_2 = 0}^{\infty} \frac{(-1)^{n_2}(n_2 + 0.5)}{(n_2 + 0.5)^2 \pi^2 + (a - s_2 t_2)^2} ds_2 , \tag{4.12}$$

interchanging the sequence of summation and integration for the variable s_2 we get

$$F_{ch2}(s_1, t_2, a) = \frac{e^a}{2j} \sum_{n_2=0}^{\infty} (-1)^{n_2}(n_2 + 0.5)I_{2n} \; , \tag{4.13}$$

where I_{2n} is

$$I_{2n} = \int_{\gamma_2 - j\infty}^{\gamma_2 + j\infty} \frac{F(s_1, s_2)}{(n_2 + 0.5)^2 \pi^2 + (a - s_2 t_2)^2} ds_2$$

$$= \int_{\gamma_2 - j\infty}^{\gamma_2 + j\infty} \frac{F(s_1, s_2)}{G_{2n}(s_1, s_2)} ds_2 = \int_{\gamma_2 - j\infty}^{\gamma_2 + j\infty} H_{2n}(s_1, s_2) ds_2 \; , \tag{4.14}$$

while, for this integral, we consider s_1 a constant parameter and s_2 as a variable. To evaluate this integral we complete the integration path by a semi-circle with an infinite radius, where the function $F(s_1, s_2)$ equals zero along this semi-circle. Using the residual theorem the result of I_{2n} is equal to the sum of the residua of $H_{2n}(s_1, s_2)$ in the poles lying inside the integration contour multiplied by $2\pi j$ [5]. In our case the poles of $H_{2n}(s_1, s_2)$ are formed by poles of $F(s_1, s_2)$ and roots of $G_{2n}(s_1, s_2)$, see (4.14). On principle, the poles of $F(s_1, s_2)$ lay on the left side of the Gaussian plane, because $F(s_1, s_2)$ represents mainly stable systems, whereas the roots of $G_{2n}(s_1, s_2)$ lay on the right side of the complex plane, namely

$$s_{21} = \frac{a + j(n_2 + 0.5)\pi}{t_2}, \;\; s_{22} = \frac{a - j(n_2 + 0.5)\pi}{t_2}. \tag{4.15}$$

The process we follow when applying the residual theorem is to choose the contour of integration around the poles of $H_{2n}(s_1, s_2)$, i.e. the roots of $G_{2n}(s_1, s_2)$, while multiplying the result by minus $2\pi j$. The reason of multiplying by minus sign is due to integrating in a mathematically opposite direction, we integrate on the right side of the complex plane. Solving for I_{2n} and substituting back to (4.13) we get

$$F_{ch2}(s_1, t_2, a) = -\frac{e^a}{t_2} \sum_{n_2=0}^{\infty} (-1)^{n_2} \text{Im} \left\{ F\left(s_1, \left[\frac{a + j(n_2 + 0.5)\pi}{t_2}\right]\right) \right\}. \tag{4.16}$$

Performing the 2$^{\text{nd}}$ partial i.L.t. with respect to s_1 and considering t_2 here to be a parameter we get

$$f_{ch}(t_1, t_2, a) = \frac{-e^{2a}}{2j t_2} \int_{\gamma_1 - j\infty}^{\gamma_1 + j\infty} \left(\sum_{n_2=0}^{\infty} (-1)^{n_2} \text{Im} \left\{ F\left(s_1, \left[\frac{a}{t_2} + j(n_2 + 0.5)\frac{\pi}{t_2}\right]\right) \right\} \right) \cdots$$

$$\times \left(\sum_{n_1=0}^{\infty} \frac{(-1)^{n_1}(n_1 + 0.5)}{(n_1 + 0.5)^2 \pi^2 + (a - s_1 t_1)^2} \right) ds_1 \; . \tag{4.17}$$

Interchanging the sequence of summation and integration,

$$f_{ch}(t_1, t_2, a) = \frac{-e^{2a}}{2j t_2} \sum_{n_1=0}^{\infty} \sum_{n_2=0}^{\infty} (-1)^{n_2} \int_{\gamma_1 - j\infty}^{\gamma_1 + j\infty} \text{Im} \left\{ F\left(s_1, \left[\frac{a}{t_2} + j(n_2 + 0.5)\frac{\pi}{t_2}\right]\right) \right\} \cdots$$

$$\times \left(\frac{(-1)^{n_1}(n_1 + 0.5)}{(n_1 + 0.5)^2 \pi^2 + (a - s_1 t_1)^2} \right) ds_1 \; , \tag{4.18}$$

$$f_{ch}(t_1, t_2, a) = \frac{-e^{2a}}{2j t_2} \sum_{n_1=0}^{\infty} \sum_{n_2=0}^{\infty} (-1)^{n_2}(-1)^{n_1}(n_1 + 0.5)I_{n_1} \; , \tag{4.19}$$

where I_{n_1} is

$$I_{n_1} = \int_{\gamma_1 - j\infty}^{\gamma_1 + j\infty} \frac{\text{Im}\{F(s_1, [\frac{a}{t_2} + j(n_2 + 0.5)\frac{\pi}{t_2}])\}}{(n_1 + 0.5)^2\pi^2 + (a - s_1 t_1)^2} \, , \qquad (4.20)$$

now, similarly as done for the first partial i.L.t., i.e. evaluating the integral by completing the integration path on a semi-circle with an infinite radius and using the residual theorem and then performing some mathematical manipulations the resulting approximate algorithm is, [26],

$$f_{ch}(t_1, t_2, a) = \frac{e^{2a}}{t_1 t_2} \sum_{n_1=0}^{\infty} \sum_{n_2=0}^{\infty} (-1)^{n_1+n_2} \cdots$$
$$\times \text{Im}\left\{ F\left(\frac{[a + j(n_1 + 0.5)\pi]}{t_1}, \frac{[a + j(n_2 + 0.5)\pi]}{t_2} \right) \right\} , \quad (4.21)$$

noting that the parameter a can be same or different valued for each variable, which can help optimize the results. Furthermore, we continue with the 2D expansion of the second i.L.t. Bromwich integral exponential kernel, i.e. the $E_{sh}(st, a)$ part. Henceforth, the reciprocal hyperbolic function appearing in $E_{sh}(st, a)$ is expressed by the infinite sum of rational functions

$$\frac{1}{\sinh z} = \frac{1}{z} + 2z \sum_{n=1}^{\infty} \frac{(-1)^n}{n^2\pi^2 + z^2}, \qquad (4.22)$$

Replacing both exponential kernels that appear in the double integral (4.3), by their respective approximations E_{sh2} and E_{sh1}, we get

$$E_{sh2}(s_2 t_2, a) = e^{2a} \left[\frac{1}{2(a - s_2 t_2)} + (a - s_2 t_2) \sum_{n_2=1}^{\infty} \frac{(-1)^{n_2}}{n_2^2\pi^2 + (a - s_2 t_2)^2} \right] , \qquad (4.23)$$

$$E_{sh1}(s_1 t_1, a) = e^{2a} \left[\frac{1}{2(a - s_1 t_1)} + (a - s_1 t_1) \sum_{n_1=1}^{\infty} \frac{(-1)^{n_1}}{n_1^2\pi^2 + (a - s_1 t_1)^2} \right] , \qquad (4.24)$$

Afterwards, following similar process as done for the first derivation i.e. from (4.12) to (4.21), namely performing the first and second partial i. L. t. with the similar assumptions and considerations, then the second approximation is obtained and the resulting algorithm is given as, [26],

$$f_{sh}(t_1, t_2, a) = \frac{e^{2a}}{2t_1 t_2} \left[\frac{1}{2} F\left(\frac{a}{t_1}, \frac{a}{t_2} \right) + \sum_{n_2=1}^{\infty} (-1)^{n_2} \text{Re}\left\{ F\left(\frac{a}{t_1}, \left[\frac{a + jn_2\pi}{t_2} \right] \right) \right\} \cdots \right.$$
$$+ \sum_{n_1=1}^{\infty} (-1)^{n_1} \text{Re}\left\{ F\left(\left[\frac{a + jn_1\pi}{t_1} \right], \frac{a}{t_2} \right) \right\} \cdots$$
$$\left. + 2 \sum_{n_1=1}^{\infty} \sum_{n_2=1}^{\infty} (-1)^{n_1+n_2} \text{Re}\left\{ F\left([\frac{a + jn_1\pi}{t_1}][\frac{a + jn_2\pi}{t_2}] \right) \right\} \right]. \quad (4.25)$$

Finally, for a higher accuracy of the method, the arithmetic mean of (4.21) and (4.25) is considered as the 2D hyperbolic NILT algorithm, and Euler transform is used to accelerate the convergence of infinite series, since it has shown the best results for the 1D hyperbolic NILT. It is worth mentioning that the original variables i.e. t_1, t_2 can be any two variables, such as time and space for instance.

4.2 Error analysis of devised 2D hyperbolic NILT method

Investigating the 2D NILT algorithm (4.21) and its derivation steps, it can be noticed that there exist two sources of errors, namely, the static error and the dynamic error [5]. The latter resulting from the practical truncation of the infinite series of the algorithm up to a certain number of terms when performing a practical computation, this error can be significantly reduced by successfully adapting suitable convergence acceleration techniques, such as those presented in Sect. 3.2 for the 1D hyperbolic NILT method. In contrast, the static error is caused by the approximation of the exponential kernel e^{st} by the proposed hyperbolic relation approximations, and this can be decreased by an optimization of the parameter a, as will be investigated in more details in this section [26].

In order to efficiently compute the static error of (4.21), first, we start by expressing the approximate kernels $E_{ch1}(s_1 t_1, a)$ and $E_{ch2}(s_2 t_2, a)$ both by an alternative manner, namely

$$e^{st} \approx E_{ch}(st, a) = \frac{e^a}{2\cosh(a - st)} = \frac{e^{st}}{1 + e^{-2a}e^{2st}}, \tag{4.26}$$

When the parameter $a > \gamma t$, it is possible to expand the fraction in (4.26) by a convergent MacLaurin series

$$E_{ch}(st, a) = e^{st} + \sum_{n=1}^{\infty} (-1)^n e^{-2na} e^{(2n+1)st}, \tag{4.27}$$

Considering the alternative approximation of the exponential kernel, and performing the first partial i.L.t. with respect to s_2 we get

$$F_{ch2}(s_1, t_2, a) = F_2(s_1, t_2) + \varepsilon_{ch2}(s_1, t_2, a), \tag{4.28}$$

where the expression $\varepsilon_{ch2}(s_1, t_2, a) = -e^{-2a}F_2(s_1, 3t_2) + e^{-4a}F_2(s_1, 5t_2) - \cdots$. Assuming $e^{-2a} << 1$ and continuing for the second partial i.L.t. with respect to s_1, the result is

$$f_{ch}(t_1, t_2, a) = f(t_1, t_2) - e^{-2a}f(t_1, 3t_2) + \sum_{n_1=1}^{\infty} \left((-1)^{n_1} e^{-2n_1 a} f([2n_1 + 1]t_1, t_2) \right) \cdots$$

$$- e^{-2a} \sum_{n_1=1}^{\infty} \left((-1)^{n_1} e^{-2n_1 a} f([2n_1 + 1]t_1, 3t_2) \right) = f(t_1, t_2) + \varepsilon_{ch}(t_1, t_2, a). \tag{4.29}$$

At this point the static error can be theoretically computed through the resulting absolute error, namely

$$\varepsilon_{ch}(t_1, t_2, a) = f_{ch}(t_1, t_2, a) - f(t_1, t_2) \approx -e^{-2a}f(3t_1, t_2) - e^{-2a}f(t_1, 3t_2)$$

$$\approx 2Me^{-2a}, \tag{4.30}$$

where M is a maximal absolute value of an original function $f(t_1, t_2)$. It is evident that the static error declines rapidly by increasing the parameter a.

In previous work [5], it was shown that the hyperbolic NILT method can be considered to behave as a low-pass filter with the cutoff frequency varying with time, i.e. $f_{\text{cut}} = \frac{n_{sum}}{2t}$. Taking this point into consideration can have a more clear understanding for the derived theoretical static error for the 2D hyperbolic NILT and its relation to the appointed number of terms and the cutoff frequency. Namely, when multiplicative constants at the variables t_i, $i = 1, 2$, increase in the error formula (4.30), its corresponding harmonic component disappears earlier. For instance, considering the approximate static error $\varepsilon_{ch}(t_1, t_2, a) = -e^{-2a}f(3t_1, t_2) - e^{-2a}f(t_1, 3t_2) \cdots$ when $n_{sum} = 120$ we get $t_1 = \frac{n_{sum}}{(2 \cdot 3)} = 20$ s, $t_2 = \frac{n_{sum}}{(2 \cdot 1)} = 60$ s and so on. In Table 4.1 the theoretical absolute static errors of the proposed 2D hyperbolic NILT method for some typical 2D Laplace

transforms and their known originals are shown.

Tab. 4.1: Absolute static errors of the hyperbolic 2D NILT

Function	I	II
$F(s_1,s_2)$	$\frac{1}{(s_1+1)(s_2+2)}$	$\frac{1}{((s_1+1)(s_2+1))^2}$
$f(t_1,t_2)$	$e^{-t_1-2t_2}$	$t_1 t_2 e^{-(t_1+t_2)}$
Abs.error	$-e^{-(3t_1+2t_2+2a)}-e^{-(t_1+6t_2+2a)}$	$-3t_1 t_2 e^{-2a}\left(e^{-(3t_1+t_2)}+e^{-(t_1+3t_2)}\right)$

In the next section, the developed 2D hyperbolic NILT accelerated with Euler transform is compared with some other available 2D NILT methods as for their accuracy and computational efficiency. As these compared methods do not have any open access program codes available for use, thus, they were programmed in the Matlab language in order to fairly test them.

4.3   Comparative analysis of the 2D hyperbolic NILT method

The developed 2D hyperbolic NILT method under discussion is compared with two other methods; namely, the 2D NILT method from K. Singhal et al. [14], and the 2D-NILT proposed by M. Moorthy [54]. To evaluate the accuracy, the ζ_2 measure with a grid of 64×64 points is used, and is expressed as follows

$$\zeta_2 = \sqrt[2]{\sum_{i=1}^{64}\sum_{j=1}^{64}\frac{\left[f(t_{1i},t_{2j})-\hat{f}(t_{1i},t_{2j})\right]^2}{(64 \times 64)}} \tag{4.31}$$

where f is the original function and $\hat{f}$ is the corresponding 2D-NILT result. Three test functions with known originals are used for the accuracy test; namely,

- $F_1(s_1,s_2) = [(s_1^2+1)(s_2^2+1)]^{-1} \;\to\; f_1(t_1,t_2) = \sin(t_1)\sin(t_2)$,

- $F_2(s_1,s_2) = (s_1+s_2)[(s_1^2+1)(s_2^2+1)]^{-1} \;\to\; f_2(t_1,t_2) = \sin(t_1)\cos(t_2)$, and

- $F_3(s_1,s_2) = (s_2^2-1)[(s_1+0.2)^2+1]^{-1}(s_2^2+1)^{-2} \;\to\; f_3(t_1,t_2) = t_2 e^{-0.2t_1}\sin(t_1)\sin(t_2)$.

Respective accuracy results for each of the 2D NILT methods, using the test functions F_1, F_2 and F_3, are shown in Table 4.2.

Tab. 4.2: Accuracy measures of 2D NILT methods using three test functions

2D NILT Method	F_1	F_2	F_3
Proposed	$2.33 \cdot 10^{-1}$	0.462	0.233
2D Singhal-NILT	$1.56 \cdot 10^{-3}$	0.499	0.291
2D Moorthy-NILT	0.6706	0.984	0.124

5 APPLICATIONS OF MNILT METHODS IN THE FIELD OF ELECTRICAL ENGINEERING

The multidimensional NILT (MNILT) methods have some potential advantages, in contrast to the 1D NILT method, which lay on the type of applications that can be solved, e.g. nonlinear circuit solution, and the ability of solving systems mathematically described by two variables, such as continuous space-time related systems. Moreover, using MNILT applications described by more than two variables can be solved, for example using 3D NILT to solve nearly nonlinear systems usinng Volterra series expanssion. The following sections are structured as follows: first the application of 2D hyperbolic NILT on simulating a lossy TL is presented [26], second a possibility of simulating weakly nonlinear circuit via MNILT methods [55].

5.1 Transmission line simulation using the 2D hyperbolic NILT method

Here, the 2D hyperbolic NILT method will be used to simulate voltage/current distributions along the TLs, as shown on a Laplace-domain TL model in Fig. 5.1 [26, 56].
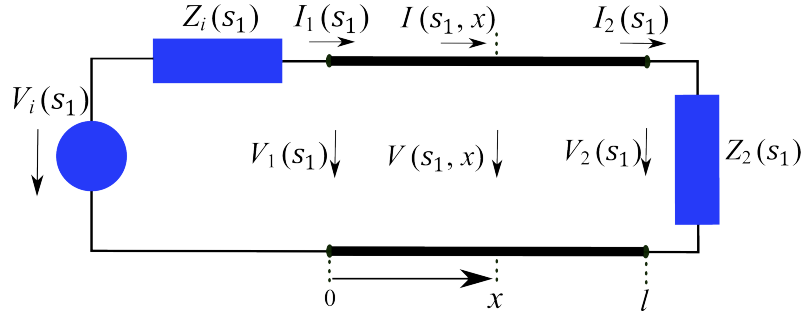

Fig. 5.1: Transmission line model in Laplace-domain with respect to the time variable.

As it is known, a TL can be described mathematically by a pair of partial differential equations (telegraphic equations) of the form

$$ -\frac{\partial v(t,x)}{\partial x} = R_0 i(t,x) + L_0 \frac{\partial i(t,x)}{\partial t} \quad , -\frac{\partial i(t,x)}{\partial x} = G_0 v(t,x) + C_0 \frac{\partial v(t,x)}{\partial t} \ ; \tag{5.1} $$

the Laplace-domain TL model in Fig. 5.1 results from the application of the Laplace transform, with respect to time, on the set of telegraphic equations (5.1), which is also represented by the equations (3.3) and (3.4) given in Chapt. 3; henceforth, these equations can be further simplified by transforming them not only with respect to the time t, but also with respect to the geometric coordinate x, resulting with fully algebraic equations,

$$ V(s,q) = \frac{qV_1(s) - \gamma(s)Z_c(s)I_1(s)}{q^2 - \gamma^2(s)} \ , \tag{5.2} $$

$$ I(s,q) = \frac{qI_1(s) - \frac{\gamma(s)}{Z_c(s)}V_1(s)}{q^2 - \gamma^2(s)} \ , \tag{5.3} $$

where zero initial conditions is considered and the boundary conditions are incorporated based on the terminating circuits. $Z_c(s_1)$ and $\gamma(s_1)$ are the characteristic impedance and the propagation

constant, respectively. $V_1(s_1)$ and $I_1(s_1)$ are given as follows

$$V_1(s_1) = V_i(s_1)\frac{Z_c(s_1)}{Z_i(s_1) + Z_c(s_1)} \cdot \frac{1 + \rho_2(s_1)e^{-\gamma(s_1)2l}}{1 - \rho_1(s_1)\rho_2(s_1)e^{-2\gamma(s_1)l}} \tag{5.4}$$

$$I_1(s_1) = V_i(s_1)\frac{1}{Z_i(s_1) + Z_c(s_1)} \cdot \frac{1 - \rho_2(s_1)e^{-\gamma(s_1)2l}}{1 - \rho_1(s_1)\rho_2(s_1)e^{-2\gamma(s_1)l}}. \tag{5.5}$$

where $\rho_1(s_1)$ and $\rho_2(s_1)$ are reflection coefficients at the beginning and end of the TL respectively. It is evident from the devised TL equations that the solution in the original domain is not possible to obtain analytically, though it is feasible by utilizing the 2D hyperbolic NILT method, and hence obtaining the simulations of the voltage/current waveform distributions along the TL numerically.

5.1.1 Transmission line via 2D hyperbolic NILT case study

As an example let us consider a TL, as in Fig. 5.1., with length of $l = 1$ m [26]. The TL is characterized by the following p.u.l. parameters: $R_0 = 1$ mΩ/m, $L_0 = 600$ nH/m, $G_0 = 2$ mS/m, $C_0 = 80$ pF/m. The TL is terminated by the impedances $Z_i = 10$ Ω, $Z_2 = 1$ kΩ. The TL is excited with the source voltage waveform:

$$v_i(t) = \begin{cases} \sin^2\left(\frac{\pi t}{2 \cdot 10^{-9}}\right), & \text{for } 0 \le t \le 2 \cdot 10^{-9}. \\ 0, & \text{otherwise.} \end{cases} \tag{5.6}$$

The voltage waveform (5.6) has the corresponding Laplace-domain transform: $V_i(s_1) = \frac{2\pi^2[1-\exp(-2\cdot10^{-9}s_1)]}{s_1[(2\cdot10^{-9}s_1)^2+4\pi^2]}$. After undergoing the 2D hyperbolic NILT the simulation results of the voltage/current propagation profiles along the TL are shown, respectively, in Fig. 5.2 and Fig. 5.3.
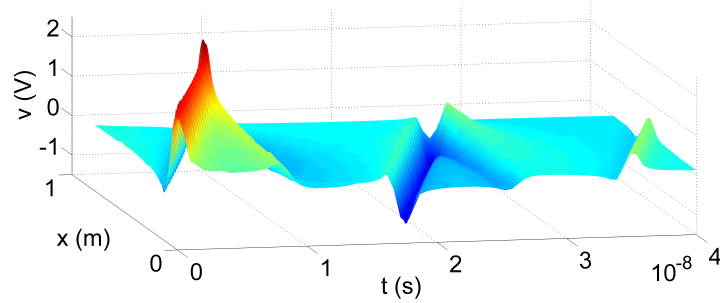

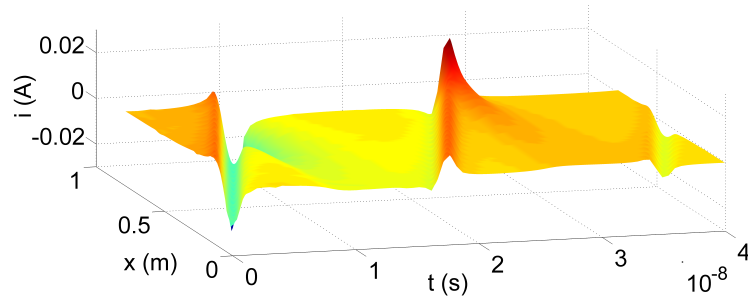Fig. 5.2: Voltage distribution along the TL via 2D hyperbolic NILT.

Fig. 5.3: Current distribution along the TL via 2D hyperbolic NILT.

5.2 Weakly nonlinear-circuit solution via MNILT

Predicting the response of nonlinear systems has been a challenge for scientists and researchers alike for many years, due to the analytical difficulties in analysing such systems. The significant importance of analysing nonlinear systems mainly arrises due to the fact that, in the physical world, several systems are to some extent nonlinear ones. In this section, it will be demonstrated the possibility of utilizing a MNILT method for the simulation of nonlinear networks based on a classical approach of Volterra series expansion [55]. There exist several approaches to solve and analyze nonlinear circuits; these approaches are based mainly on specific numerical techniques that can solve nonlinear differential equations. When considering a weakly nonlinear system, a method based on Volterra series expansion can mathematically describe the system accurately enough from a practical point of view. Nevertheless, the main limitation of this approach lies on the difficulty of obtaining the time domain results, and hence comes the advantage of using an MNILT method.

A weakly nonlinear circuit has a leverage that it can be described by third order Volterra kernels with a very reasonable accuracy. Another advantage is based on the fact that these Volterra kernels can be experimentally obtained by measuring the X-parameters through the use of a nonlinear vector network analyzer (NVNA) and afterwards transferring the results properly [55, 57]. In theory, the process of the solution is as follows: By utilizing the multidimensional Laplace transform (MLT) of a time domain nonlinear impulse response a result is a respective Laplace domain transfer function, and this, in fact, helps to obtain the needed Volterra kernels [58], by using, for example, a harmonic input method [59]. Then, after solving the system in the Laplace domain, the final step is to transfer the solution back into the time domain. This process will be mathematically shown in more detail in this section.
Assuming a response $y(t)$ to a stimulus $x(t)$ [60], has the form

$$y(t) = \sum_{n=1}^{\infty} y_n(t) \ , \tag{5.7}$$

the infinite sum has the following terms

$$y_n(t) = \int_{-\infty}^{\infty} \xrightarrow{n\text{-fold}} \int_{-\infty}^{\infty} h_n(\tau_1, \tau_2, \cdots, \tau_n) \prod_{i=1}^{n} x(t - \tau_i) d\tau_i \ , \tag{5.8}$$

with $h_n(\tau_1, \tau_2, \cdots, \tau_n)$ representing a nonlinear impulse response, also known as the n-th order Volterra kernel. These equations are shown more clearly as a flow chart in Fig. 5.4. In order to perform the Laplace-domain approach new variables are introduced by $t_1 = t_2 = \cdots = t_n = t$, and then an n-dimensional Laplace transform is applied transforming the n-fold convolution integral (5.8) into a multidimensional Laplace-domain response [58],

$$Y_n(s_1, s_2, \cdots, s_n) = H_n(s_1, s_2, \cdots, s_n) \prod_{i=1}^{n} X(s_i) \ , \tag{5.9}$$

with $H_n(s_1, s_2, \cdots, s_n)$ as a nonlinear transfer function, which can be solved for some nonlinear circuit using for instance the harmonic input method [61]. At this point the time-domain terms $y_n(t_1, t_2, \cdots, t_n)$ can be obtained by an n-D ILT, while considering $t_1 = t_2 = \cdots = t_n = t$ in the final results; a graphical representation is shown in Fig. 5.4. As we are limiting our computations to weakly nonlinear networks, i.e. considering Volterra series expansion up to the 3rd order, thus the NILTs of 1D, 2D and 3D are needed to get the required time-domain response; for more clarity, a block diagram of this process is depicted in Fig. 5.4.
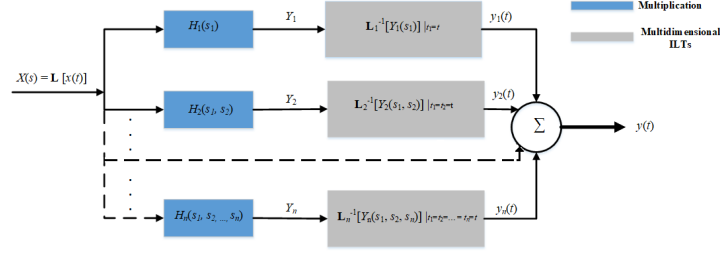
Fig. 5.4: Diagram of a nonlinear circuit solution by using Volterra series expansion and multidimensional ILTs.

5.2.1 Weakly nonlinear circuits using 1D to 3D NILTs case study

To demonstrate the approach presented in Sect. 5.2, a solution of a weakly nonlinear circuit by using 1D, 2D and 3D NILTs is presented. Let us consider a nonlinear serial LR circuit, see Fig. 5.5 [55]. The network consists of a linear inductor L, a linear resistor R, and a nonlinear resistive element R_n, the network is excited by the voltage source $v_i(t)$. Assuming square nonlinearity, i.e. the resistive element R_n having a quadratic characteristics: $v_{Rn}(t) = R_n i^2(t)$.
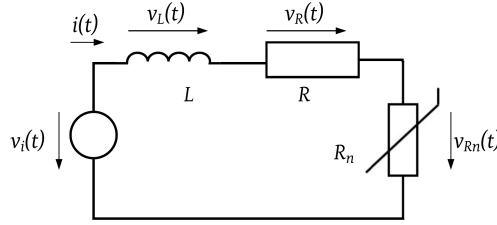

Fig. 5.5: Electrical circuit with nonlinear resistive element R_n.

In light of the foregoing, the first-order nonlinear ordinary differential equation (NODE) is given as follows,

$$L\frac{di(t)}{dt} + Ri(t) + R_n i^2(t) = v_i(t) .$$

(5.10)

In association with the block diagram in Fig. 5.4, it can be noticed that the excitation voltage $v_i(t)$ and the current $i(t)$ represent the stimulus $x(t)$ and the response $y(t)$, accordingly. Henceforth, with respect to (5.9), and assuming a third-order expansion, the following Laplace-domain partial solutions ought to be resolved,

$$I_1(s_1) = H_1(s_1)V_i(s_1),$$ (5.11a)

$$I_2(s_{1,2}) = H_2(s_1, s_2)V_i(s_1)V_i(s_2),$$ (5.11b)

$$I_3(s_1, s_2, s_3) = H_3(s_1, s_2, s_3)V_i(s_1)V_i(s_2)V_i(s_3) .$$ (5.11c)

With the use of a suitable method, for e.g. here the harmonic input method is used, and hence, the transfer functions (5.11) are solved,

$$H_1(s_1) = \frac{1}{s_1 L + R} ,$$ (5.12a)

$$H_2(s_1, s_2) = -R_n H_1(s_1)H_1(s_2)H_1(s_1 + s_2) ,$$ (5.12b)

$$H_3(s_1, s_2, s_3) = -\frac{R_n}{3}[H_1(s_1)H_2(s_2, s_3) + H_1(s_2)H_2(s_1, s_3) \cdots$$
$$+ H_1(s_3)H_2(s_1, s_2)]H_1(s_1 + s_2 + s_3) .$$ (5.12c)

37

Suppose that an exponential pulse is chosen as the excitation voltage source $v_i(t)$, with its Laplace transform given as follows,

$$v_i(t) = V_0 e^{-at} \underline{1}(t) \xrightarrow{\mathbf{L}\{\,.\,\}} V_i(s) = \frac{V_0}{s+a} \; , \tag{5.13}$$

where $a \geq 0$, and then substituting (5.13) back into (5.11), solving the respective sub-equations. The Laplace-domain responses will undergo the 1D, 2D and 3D NILT methods to obtain the resultant time-domain current response, namely,

$$\begin{aligned} i(t) &= \mathbf{L}_1^{-1}[I_1(s_1)]|_{t_1=t} + \mathbf{L}_2^{-1}[I_2(s_1,s_2)]|_{t_1=t_2=t} + \mathbf{L}_3^{-1}[I_3(s_1,s_2,s_3)]|_{t_1=t_2=t_3=t} \\ &= i_1(t_1)|_{t_1=t} + i_2(t_1,t_2)|_{t_1=t_2=t} + i_3(t_1,t_2,t_3)|_{t_1=t_2=t_3=t} \\ &= i_1(t) + i_2(t) + i_3(t) \; . \end{aligned} \tag{5.14}$$

For the simulation tests, the following parameters are considered: $L = 100$ mH, $R = 100$ mΩ, $R_n = 100$ mΩA^{-1}, $V_0 = 10$ mV, and $a = 1$. The results are illustrated in Fig. 5.6 and Fig. 5.7, showing individual terms $i_i(t)$, namely: $i_1(t)$, $i_2(t)$, and $i_3(t)$, respectively. Two cases are simulated first is with $a = 1$ (an exponential impulse), and the second one with $a = 0$ (a unit step), see (5.13), where the results are depicted in Fig. 5.6 and Fig. 5.7, respectively.

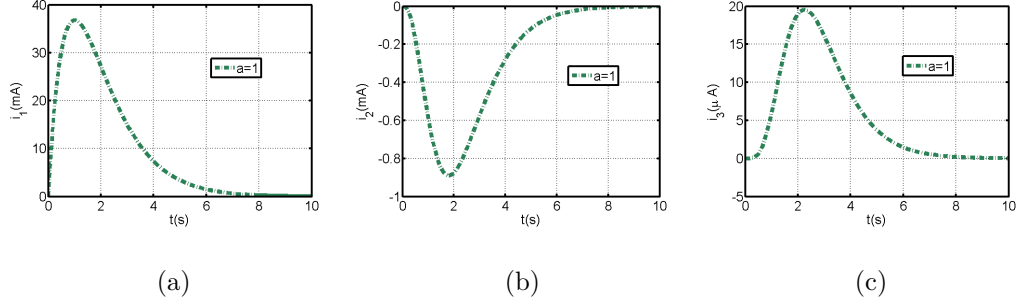Fig. 5.6: Numerical inversions leading to current response Volterra series terms by (a) 1D NILT, (b) 2D NILT, (c) 3D NILT, for an exponential impulse.
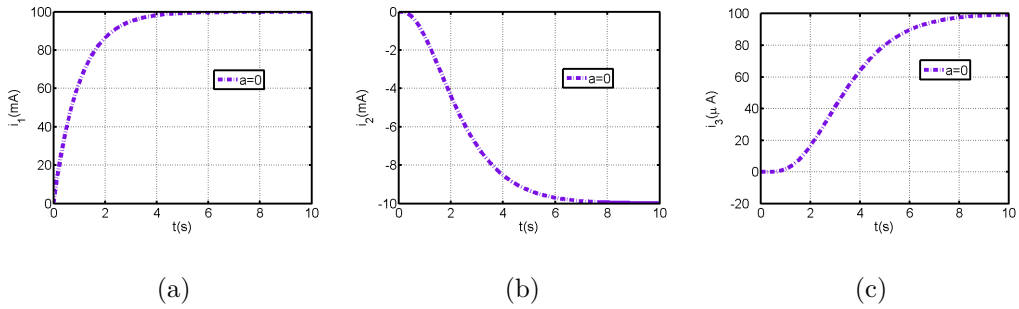

Fig. 5.7: Numerical inversions leading to current response Volterra series terms by: (a) 1D NILT, (b) 2D NILT, (c) 3D NILT, for a unit step.

The resultant current responses, computed according to (5.14), are depicted in Fig. 5.8, for both cases accordingly.
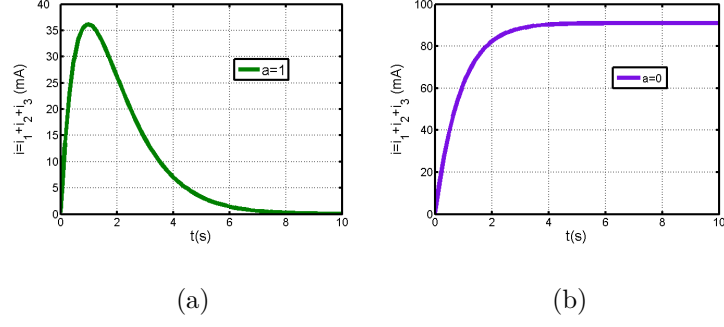
Fig. 5.8: Resulting current response for: (a) an exponential impulse, (b) a unit step.

Furthermore, the resulting current responce is computed, and the accuracy of the method, considering the exponential input case $a = 1$, is verified by comparing the resultant current response of NODE, in (5.10), computed by a Matlab built-in function, particularly, the ODE45 Runge-Kutta function, which is applied directly to the NODE, and then analyzing the relative errors, the results are shown in Fig. 5.9 [55].
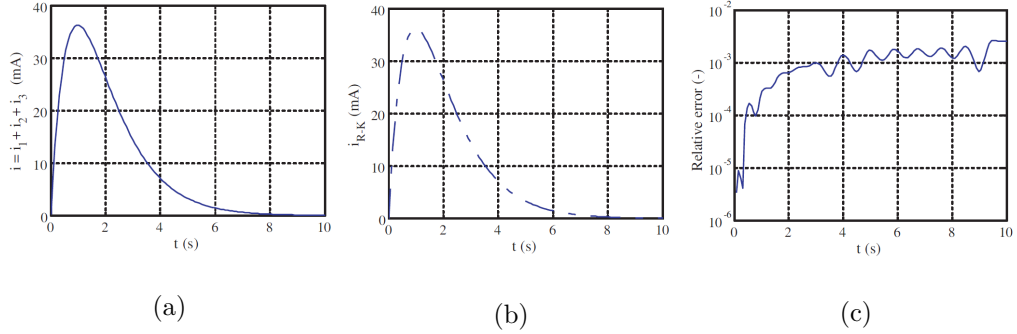
Fig. 5.9: Resultant current responce for the case $a = 1$ by: (a) Volterra series solution, (b) Runge-Kutta method, and (c) the relative error.

The simulation results were obtained using Matlab language on a common PC, and the CPU computation times were generally less than one min, while considering 64 points of time division. The 1D NILT up to 3D NILT programming codes used are available in [55].

6 RESEARCH CHALLENGES AND CONCLUSION

In this chapter, the conclusions of the doctoral thesis are presented and summarized. The main goals can be listed as follows:

- Research and development of effective NILT methods.
- Development of a promising 1D NILT method, including the detailed study of its error analysis and its successful program implementation and verification.
- Enhancements on the NILT method by incorporating different infinite series convergence acceleration techniques.
- Expansion of the proposed hyperbolic NILT method to a higher dimension, including detailed error analysis and program implementation.
- Experimental implementation of the developed NILT methods on different potential electrical engineering topics, such as the solution of ODE, PDE and even weakly nonlinear systems via MNILT method.
- Incorporating fractional-order calculus on the different NILT method field of applications.

In the first chapter, several 1D NILT methods have been tested and analyzed, mainly, regarding their accuracy, computation speed and the types of functions supported. It is clear that most available NILT methods are based on the necessity that the inverse transform of polynomial time functions up to a specific and relatively high power is accurate. Moreover, most of the available methods suffer from some limitations such as the accuracy of the method itself, the range of different functions that can be correctly inverted and the large computational time (see practical accuracy results in Fig. 2.6 and Fig. 2.7). Based on the findings, a proposed hyperbolic NILT technique that differs from other similar algorithms, namely, by reacting as a nearly ideal low pass filter with time-variable cutoff frequency, was developed and generalized. Mainly, this numerical method is based on approximation of the Bromwich integral exponential kernel by suitable hyperbolic approximations. Furthermore, the method was generalized by reducing the integration step, while providing higher accuracy of the results. After performing several tests on different types of functions, this numerical method has proved to yield results with a higher degree of accuracy and stability, including a wide range of types of functions that can be inverted, e.g. rational, irrational and transcendental functions in the Laplace domain; this is verified in Fig. 2.6 and Fig. 2.7. The hyperbolic NILT method is tested and compared to other highly cited 1D NILT methods. Additionally, further enhancements to the hyperbolic NILT method were performed by adapting several infinite series convergence accelerating algorithms. These algorithms include the quotient difference algorithm, the epsilon algorithm and the Euler transform. The former proved to be a method with high stability, while the latter, the Euler transform, improved the method with a much higher precise inversion accuracy (the results were depicted in Fig. 2.3 to Fig. 2.5). The 1D hyperbolic NILT, among other methods, was used in several applications in the electrical engineering and electronics field. These applications include the solution of transient processes in linear time invariant system. Once a given problem is resolved in the Laplace domain, the difficult part is to obtain the original results in the time-domain, as, analytically, it is usually impractical, hard or even impossible to obtain. Thus, using the NILT it is then possible to overcome these difficulties and obtain the required solution and simulations of these applications in the time domain. The applications that have been solved include: lossy TL, fractional-order TL, frequency dependent TL, and furthermore, an expansion to MTL with fractional-order elements. These successfully preformed simulations were presented in detail in Chapter 3. Moreover, in Chapter 4, an innovative approach to the numerical computation of the hyperbolic NILT method two-dimensional expansion was performed. The technique involves the repeated application of partial inverse Laplace transform operations. The detailed error analysis of the method was devised and studied in Section 4.2. The 2D hyperbolic NILT was verified

by utilizing it in more sophisticated applications, such as multiconductor transmission lines with simulations that contain both time and space variables obtained by a single computation step (see Fig. 5.2 and Fig. 5.3). Moreover, the nD NILT is used for potential applications such as weakly non-linear circuits, while using Volterra series method; these applications were presented and a case study was done in Chapter 5. Moreover, a novel approach of modeling some applications using the fractional-order domain, in contrast to the classical integer-orders of the electronic components, was effectively incorporated in the conducted applications in a straightforward manner. It was shown that with the benefit of utilizing the Laplace domain, it is feasible to include these fractional-order elements in the respective models, due to the advantage of obtaining the original time domain results with the different NILT methods. It was verified that including fractional-order elements in the simulation tests provides a better representation of the physical phenomena in such applications. Moreover, imposing fractional-order elements gives a higher degree of freedom for the optimization of these applications and a better control of its characteristics; such applications were simulated and the results were depicted in Chapter 3. All the results displayed in this doctoral thesis were programmed and implemented in the Matlab language package. For practical requirements, a CD is available which includes all the original programming codes along with the exercises and experiments performed in this doctoral thesis.

The original contributions to the doctoral thesis are:

- The development of a NILT method with an achievable high degree of accuracy.
- The discovery that the hyperbolic NILT method can be enhanced by adapting suitable infinite series convergence acceleration techniques, for instance, by providing an absolute error of about 10^{-8} or even less for some tested functions.
- The demonstration that the NILT method is a computationally effective method able to solve mathematical models of interconnects based on telegraphic equations or on RLCG lumped elements.
- The discovery that using the NILT method followed by the simulation of TL/MTL high-frequency losses, nonuniformity of the wires, and inclusion of fractional-order TL elements, in contrast to the conventional integer ones, can be all done in a novel and simple manner.
- Implementation of previous findings into the new developed 2D hyperbolic NILT method, followed by a detailed error analysis of the method and verification by solving practical applications in the electrical engineering field.
- Solving weakly nonlinear systems using MNILT method of up to three variables with the assistance of Volterra series expansion method.
- Optimization of the free parameter values for some 1D and 2D NILT methods.

Future work recommendations:

- Generalization of the hyperbolic 2D NILT method to three variables based on partial inversions and including the error analysis.
- Familiarization with parallel programming techniques and the possible deployment to MNILT methods.
- Programming implementations of the method and the simulation of potential applications requiring MNILTs with a possibility of modeling in the fractional-order domain.
- Possible future collaboration with the Department of Engineering Science and Mechanics, Pennsylvania State University for the application of the hyperbolic NILT method in direct and inverse heat conduction and thermoelasticity with prof. A. E. Segall.

Bibliography

[1] L. Brančík, and N. Al-Zubaidi R-Smith, "Two approaches to derive approximate formulae of NILT method with generalization," 38th *International Convention on Information and Communication Technology, Electronics and Microelectronics (MIPRO)*, Croatia, pp. 155–160, 2015.

[2] J. Toutain, J.-L. Battaglia, C. Pradere, J. Pailhes, A. Kusiak, W. Aregba, and J.- C. Batsale, "Numerical inversion of Laplace transform for time resolved thermal characterization experiment,"*Journal of Heat Transfer*, vol. 133, no. 4, ID: 044504, 2011.

[3] G. V. Milovanovic, and A. S. Cvetkovic, "Numerical inversion of the Laplace transform," *Facta. Univ. Ser. Electr. Energ.*, vol. 18, No. 3, pp. 515-530, 2005.

[4] R. G. Campos, and A. Huet, "Numerical inversion of the Laplace transform and its application to fractional diffusion,"*Journal Applied Mathematics and Computation*, vol. 327, pp. 70-78, 2018.

[5] J. Valsa, and L. Brančík, "Approximate formulae for numerical inversion of Laplace transforms,"*International Journal of Numerical Modelling: Electronic Networks, Devices and Fields*, vol. 11, pp. 153-166, 1998.

[6] G. Honig, and U. Hirdes, "A method for the numerical inversion of Laplace transforms,"*Journal of Computational and Applied Mathematics*, vol. 10, pp. 113-132, 2// 1984.

[7] T. Hosono, "Numerical inversion of Laplace transform and some applications to wave optics,"*Radio Science*, vol. 16, pp. 1015-1019, 1981.

[8] L. Brančík, "Programs for fast numerical inversion of two-dimensional Laplace transforms in Matlab language environment with some applications," *in Proceedings of the* 23rd *International Conference on Fundamentals of Electrotechnics and Circuit Theory SPETO'2000*, Gliwice-Ustroň, Poland, pp. 197-200, 2000.

[9] K. Singhal, and J. Vlach, "Computation of time domain response by numerical inversion of the Laplace transform,"*Journal of the Franklin Institute*, vol. 299, pp. 109-126, 2// 1975.

[10] L. Brančík, "An improvement of FFT-based numerical inversion of two-dimensional Laplace transforms by means of ϵ-algorithm,"*in Proceedings of IEEE ISCAS'2000*, Geneva, Switzerland, pp. 581-584, 2000.

[11] A. M. Cohen, *Numerical methods for Laplace transform inversion*, New York, N.Y: Springer, 2007.

[12] J. Abate, G. L. Choudhury, and W. Whitt, "Numerical inversion of multidimensional Laplace transforms by the Laguerre method,"*Performance Evaluation*, vol. 31, pp. 229-243, 1// 1998.

[13] L. Brančík, "Numerical Inverse Laplace Transforms for Electrical Engineering Simulation,"*in MATLAB for Engineers-Applications in Control, Electrical Engineering, IT and Robotics*, Edited by Karel Perutka, Rijeka: InTech, pp. 51-74, 2011.

[14] K. Singhal, J. Vlach, and M. Vlach, "Numerical inversion of multidimensional Laplace transform,"*Proceedings of the IEEE*, vol. 63, pp. 1627-1628, 1975.

[15] P. P. Valkó, and J. Abate, "Numerical inversion of 2-D Laplace transforms applied to fractional diffusion equations,"*Applied Numerical Mathematics*, vol. 53, pp. 73-88, 4// 2005.

[16] P. Gomez, L. Vergara, R. Nuricumbo-Guillen, and F. P. Espino-Cortes, "Two-Dimensional Definition of the Numerical Laplace Transform for Fast Computation of Transient Profiles Along Power Transmission Lines," *IEEE Transactions on Power Delivery*, vol. 31, pp. 412-414, 2016.

[17] L. Brančík, and N. Al-Zubaidi R-Smith, "Commentary on method of numerical inverse Laplace transformation - possible generalization and error analysis," *in Electronic Horizon*, vol. 70, no. 4, pp. 6-10, 2014.

[18] N. Al-Zubaidi R-Smith, and L. Brančík, "Comparative study on one-dimensional numerical inverse Laplace transform methods for electrical engineering," *in Elektrorevue e-journal*, vol. 18, no. 1, pp. 1-8, 2016.

[19] P. Wynn, "A note on the generalized Euler transformation," *Computer Journal*, vol. 14, pp. 437-441, 1971.

[20] P. Henrici, "Quotient-difference algorithms," *in Mathematical Methods for Digital Computers*,vol. 2, A. Ralston and H. S. Wilf, eds., J. Wiley, N. York, pp. 37-62, 1967.

[21] H. Rutishauser *Der Quotienten-Differenzen-Algorithmus*, Basel, Birkhauser Verlag, 1957.

[22] L. Brančík, "Technique of 3D NILT based on complex Fourier series and quotient-difference algorithm," 17th *IEEE Int. Conference on Electronics, Circuits, and Systems (ICECS)*,Athens, pp. 203-206, 2010.

[23] J. R. Macdonald, "Accelerated convergence, divergence, iteration, extrapolation, and curve fitting," *Journal Applied Physics*,vol.10, pp. 3034-3041, 1964.

[24] N. Al-Zubaidi R-Smith, and L. Brančík, "Convergence acceleration techniques for proposed numerical inverse Laplace transform method," 24th *Telecommunications Forum (TELFOR)*, Belgrade, Serbia, IEEE, pp. 1-4, 2016.

[25] P. Wynn, "The epsilon algorithm and operational formulas of numerical analysis," *Mathematics of Computation*, vol.15, no.74, pp. 151-158, 1961.

[26] N. Al-Zubaidi R-Smith, and L. Brančík, "Proposed hyperbolic NILT method—acceleration techniques and two-dimensional expansion for electrical engineering applications," *IEICE Transactions on Fundamentals of Electronics, Communications and Computer Sciences*, vol. E101-A, no.5, pp. 763-771, 2018.

[27] V. Zakian, "Numerical inversion of Laplace transform,"*Electronics Letters*, vol. 5, pp. 120-121, 1969.

[28] J. A. C. Weideman, "Optimizing Talbot's Contours for the Inversion of the Laplace Transform," *SIAM Journal on Numerical Analysis*, vol. 44, pp. 2342-2362, 2006.

[29] H. Stehfest, "Algorithm 368: Numerical inversion of Laplace transforms [D5],"*Communications of the ACM*, vol. 13, pp. 47-49, 1970.

[30] L. Brančík, "Utilization of quotient-difference algorithm in FFT based numerical ILT method,"*in Proceedings of the 11th International Czech-Slovak Scientific Conference Radioelektronica 01*, Brno, Czech Republic, pp. 352-355, 2001.

[31] Y. Feng, W. Xinhai, and L. Hong, "Application of Laplace transform in well test interpretation - an example of the oilfield cavity-fractured reservoirs in tarim basin," *in International Conference on Multimedia Technology (ICMT)*, pp. 1988-1991, 2011.

[32] J. A. T. Machado, V. Kiryakova, and F. Mainardi, "Recent history of fractional calculus," *Communications in Nonlinear Science and Numerical Simulation*, vol. 16, no. 3, pp. 1140-1153, 2011.

[33] R. E. Gutierrez, J. M. Rosario, and J. T. Machado, "Fractional order calculus: basic concepts and engineering applications," *Mathematical Problems in Engineering*, vol. 2010, Article ID 375858, 19 pages, 2010.

[34] K. Oldham, and J. Spanier, *The Fractional Calculus: Theory and Applications of Differentiation and Integration to Arbitrary Order*, (New York: Academic Press, 1974).

[35] M. Meerschaert, and A. Sikorskii, *Stochastic Models for Fractional Calculus*, Berlin, Germany: De Gruyter, 2011.

[36] R. Ismail, and R. A. El-Barkouky, "Fractional-order transmission line modeling," *International Journal of Advances in Computer Science and Technology IJACST*, vol. 2, no. 11, pp. 18-24, 2013.

[37] N. Al-Zubaidi R-Smith, A. Kartci, and L. Brančík, "Fractional-order lossy transmission line with skin effect using NILT method," *Proceedings of the 40th International Conference on Telecommunications and Signal Processing TSP*, Barcelona, Spain,, pp.730-734, 2017.

[38] N. Nahman, and D. Holt, "Transient analysis of coaxial cables using the skin effect approximation," *Circuit Theory, IEEE Transactions*, vol. 19, no. 5, pp. 443-451, 1972.

[39] C. R. Paul, *Analysis of Multiconductor Transmission Lines*, John Wiley and Sons, New York, 1994.

[40] N. Al-Zubaidi R-Smith, "Accelerated hyperbolic NILT method used for frequency-dependent transmission line simulation," *Proceedings of the 23rd Conference Student EEICT*, Brno University of Technology, Brno, Czech Republic, pp. 634 – 639, 2017.

[41] N. Al-Zubaidi R-Smith, A. Kartci, and L. Brančík, "Application of Numerical Inverse Laplace Transform Methods for Simulation of Distributed Systems with Fractional-Order Elements," *Journal of Circuits, Systems, and Computers JCSC*, vol. 27, no. 11, pp 1-25. 2018.

[42] J. A. B. Faria, *Multiconductor Transmission-Line Structures: Modal Analysis Techniques*, John Wiley and Sons, New York, 1993.

[43] L. Brančík, and B. Ševčík, "Computer simulation of nonuniform MTLs via implicit Wendroff and state-variable methods," *Radioengineering*, vol. 20, no. 1, pp. 221-227, 2011.

[44] L. Brančík, "Improved method of numerical inversion of two-dimensional Laplace transforms for dynamical systems simulation," *Proceedings of the 9th IEEE ICECS'02*, Dubrovnik, Croatia, pp. 385-88, 2002.

[45] L. Brančík, "Simulation of multiconductor transmission lines using two-dimensional Laplace transformation," *Proceedings of the 15th European Conference Circuit Theory and Design ECCTD'01*, Espoo, Finland, pp. 133-136, 2001.

[46] M. Ortigueira, *Fractional Calculus for Scientists and Engineers*, Springer, 2011.

[47] Z. Yanzhu, and X. Dingyu, "Dynamical simulation analysis based on time fractional transmission line model," 7th *International Symposium on Antennas, Propagation and EM Theory, ISPE'06*, Guilin, China, pp. 1-4, 2006.

[48] O. P. Agrawal, "A general solution for a fourth-order fractional diffusion-wave equation defined in a bounded domain," *Computers and Structures*, vol. 79, no. 16, 1497-1501, 2001.

[49] L. Brančík, "The fast computing method of numerical inversion of Laplace transforms using FFT algorithm," *in Proceedings of the 5th EDS 98 International Conference*, Brno, Czech Republic, pp. 97-100, 1998.

[50] J. Valsa, "Numerical inversion of multivariable Laplace transforms," *Proceedings of the 5th Electronic Devices and Systems International Conference EDS98*, Brno, Czech Republic, pp. 337-340, 1998.

[51] V. A. Ditkin, and A. P. Prudnikov, *Operational Calculus in Two Variables and its Applications*, New York, Pergamon, 1962.

[52] L. Brančík, "Numerical Inversion of Two-Dimensional Laplace Transforms Based on Partial Inversions," *in Proceedings of the 17th International Conference Radioelektronika'07*, Brno, Czech Republic, pp. 451-454, 2007.

[53] L. Brančík, "Error analysis at numerical inversion of multidimensional Laplace transforms based on complex Fourier series approximation,"*IEICE Transactions on Fundamentals of Electronics, Communications and Computer Sciences*, vol. E94-A, no. 3, pp. 999-1001, 2011.

[54] M. V. Moorthy, "Numerical inversion of two-dimensional Laplace transforms–Fourier series representation," *Applied Numerical Mathematics*, vol. 17, pp. 119-127, 5// 1995.

[55] L. Brančík, N. Al-Zubaidi R-Smith, and F. Záplata, "Matlab Simulation of Nonlinear Electrical Networks via Volterra Series Expansion and Multidimensional NILT,"*Progress in Electromagnetic Research Symposium (PIERS)* Singapore, Singapore, pp. 2822-2829, IEEE, 2017.

[56] N. Al-Zubaidi R-Smith, and L. Brančík, "On two-dimensional numerical inverse Laplace transforms with transmission line applications," *In 2016 Progress in Electromagnetics Research Symposium (PIERS)*.Shanghai, China, pp. 227-231, 2016.

[57] L. Sang, J. Wang, Y. Xu, and R. Xu, "Extracting Volterra Series Representation from *X*-parameters for the Modeling of Microwave Device,"*Journal of Electromagnetic Waves and Applications,* vol. 27, no. 3, 299-308, 2013.

[58] S. B. Karmakar, "Laplace transform solution of nonlinear differential equations," *Indian Journal of Pure and Applied Mathematics,* vol. 11, no. 4, 407-412, 1980.

[59] J. Debnath, and N. C. Debnath, "Associated transforms for solution of nonlinear equations," *International Journal of Mathematics and Mathematical Sciences,* vol. 14, no. 1, 177-190, 1991.

[60] M. Schetzen, *The Volterra and Wiener Theories of Nonlinear Hybrid Systems,* Krieger Publishing Company, New York, 2006.

[61] J. J. Bussgang, L. Ehrman, and J. W. Graham, "Analysis of nonlinear systems with multiple inputs," *Proceedings of the IEEE,* vol. 62, no. 8, 1088-1119, 1974.

CURRICULUM VITAE

Nawfal Al-Zubaidi R-Smith

Technicka 3082/12,
616 00, Brno
Czech Republic
Phone: +420 5 4114 6556. Mobile: +4367762681530
Email: alzubaidi@phd.feec.vutbr.cz
Email: nawfal.smith@gmail.com

RESEARCH INTERESTS

Numerical methods for electrical engineering, computer-aided simulation, signal integrity issues in electronic circuits, transmission lines and fractional calculus.

EDUCATION

Since 2014: Brno University of Technology, Brno, Czech Republic.

- Postgraduate studies at the Department of Radio Electronics, Study Programme: Electrical, Electronic, Communication and Control Technology (PhD Candidate).
- Thesis: Methods of numerical inversion of Laplace transforms for electrical engineering and their applications.

2010-2013: Blekinge Institute of Technology, Karlskrona, Sweden.

- Master of Science (MSc.), Electrical Engineering with Emphasis on Radio Communication.
- Thesis: An Efficient Scheme in IEEE 802.22 WRAN for Real Time and Non-Real Time Traffic Delay.

2004-2009: Yarmouk University, Irbid, Jordan.

- Bachelor of Science (BSc.), Electrical Engineering and Communications.
- Thesis: Ad Hoc Networks – Performance & Analysis.

ACADEMIC APPOINTMENTS	➢ Since 9/2014: Department of Radio Electronics, Brno University of Technology. ➢ 5/2013-9/2013: Research assistant, department of computer science, Aarhus University, Aarhus, Denmark.
RESEARCH STAY	➢ 4/2018 - 8/2018: Exchange Fellow at Johannes Kepler University, Linz, Austria.
COMPUTER SKILLS	➢ Matlab – Intermediate ➢ MS Office, LaTeX- Advanced ➢ OrCad PSpice, AutoCad – Intermediate ➢ Adobe InDesign – Intermediate ➢ Adobe Photoshop – Intermediate ➢ Salesforce and Siebel – Advanced
WORK & EXPERIENCE	➢ 2/2009 – 8/2009 Orange Telecommunications Co, Jordan. ➢ 2/2014 – 12/2014 Lindberg International A/S, Denmark. ➢ 2018 Zebra Technologies Europe Limited, Czech Republic.
LANGUAGE SKILLS	➢ Arabic – Native speaker. ➢ Spanish – Native speaker. ➢ English – Advanced. ➢ German – Basic knowledge. ➢ Italian – Basic Knowledge.

ACHIEVMENTS

➢ Best paper award at the 40th international conference on telecommunications and signal processing (TSP) 2017, supported by IEEE.
➢ EEICT student conference 2017 winning best work certificate for 3rd position.

ABSTRACT

Numerical inverse Laplace transform (NILT) methods have become a fundamental part of the numerical toolset of practitioners and researchers in a large number of science and engineering fields, especially in the electrical engineering applied domain. Mainly, NILT techniques assist in getting the time-domain simulations in related applications, e.g. solving ordinary differential equations as those appearing when solving lumped-parameter circuits, solving partial differential equations as in linear distributed-parameter systems or those emerging while investigating signal integrity issues.

  Generally, most available 1D NILT methods are very specific, i.e. they perform well on a few type of functions and hence on a limited number of applications; thus the aim of this research is to provide a broad treatment of such numerical methods, the development of universal NILT method and its expansion to multidimensional NILT which can cover a wide field of applications and could provide a practical mechanism for a better diagnosis and analysis of time-domain simulations. The reach of the ideas is presented by discussing a wide range of case studies and applications; for example, the NILT methods are applied in solving transmission lines, including multiconductor ones, and even for the solution of weakly non-linear circuits while utilizing multivariable NILTs. With the assistance of the NILT method an advantage of including frequency dependent parameters and using fractional-order elements in their respective models can be done in a very accurate and simple manner.